LAPPEENRANTA UNIVERSITY OF TECHNOLOGY
Faculty of Technology
LUT Mechanical Engineering
Master's Thesis

Ville Hakonen

Virtual Testing of Active Magnetic Bearing Systems based on Design Guidelines given by the Standards

Examiners: Professor Jussi Sopanen
Docent Harri Eskelinen

Supervisor: M.Sc. Janne Heikkinen

Lappeenranta, 10.11.2014

ABSTRACT

Lappeenranta University of Technology
Faculty of Technology
LUT Mechanical Engineering
Mechanical Engineering

Ville Hakonen

Virtual Testing of Active Magnetic Bearing Systems based on Design Guidelines given bt the Standards

Master's thesis
2014
78 pages, 30 figures, 9 tables and 5 appendices

Examiners: Professor Jussi Sopanen
Docent Harri Eskelinen
Supervisor: M.Sc. Janne Heikkinen

Keywords: Active Magnetic Bearing, AMB, AMB standards, AMB simulation, verification of AMB system**.**

Active Magnetic Bearings offer many advantages that have brought new applications to the industry. However, similarly to all new technology, active magnetic bearings also have downsides and one of those is the low standardization level. This thesis is studying mainly the ISO 14839 standard and more specifically the system verification methods. These verifying methods are conducted using a practical test with an existing active magnetic bearing system. The system is simulated with Matlab using rotor-bearing dynamics toolbox, but this study does not include the exact simulation code or a direct algebra calculation. However, this study provides the proof that standardized simulation methods can be applied in practical problems.

TIIVISTELMÄ

Lappeenrannan teknillinen yliopisto
Teknillinen tiedekunta
LUT Kone
Konetekniikka

Ville Hakonen

Aktiivisen magneettilaakerijärjestelmän virtuaalinen testaus käyttäen standardien määräämiä suunnittelu ohjeita

Diplomityö
2014
78 sivua, 30 kuvaa, 9 taulukkoa ja 5 liitettä

Tarkastajat: Professori Jussi Sopanen
Dosentti Harri Eskelinen
Ohjaaja: DI Janne Heikkinen

Hakusanat: Aktiivinen magneetti laakeri, AMB, AMB standardit, AMB simulointi, AMB systeemin todentaminen.
Keywords: Active Magnetic Bearing, AMB, AMB standards, AMB simulation, verification of AMB system

Aktiiviset magneettilaakerit tuovat useita uusia hyötyjä, jotka puolestaan tuovat uusia sovelluksia teollisuuteen. Kuten kaikessa uudessa tekniikassa, on aktiivissa magneettilaakereissa huonoja puolia ja yksi niistä on alhainen standardisoinnin taso. Tämä tutkimus käsittelee pääsääntöisesti ISO 14839 standardin mukaisia simulaation ja systeemin varmennusmenetelmiä. Näitä varmennusmenetelmiä tutkitaan käyttäen avuksi olemassa olevaa suunnitelmaa aktiivisesta magneettilaakerisysteemistä. Tämä systeemi mallinnetaan käyttäen Matlab ohjelmassa roottori-laakeri dynamiikka laskentaohjelmistoa, jonka avulla voidaan tutkia suhteellisen tarkasti systeemissä tapahtuvia muutoksia. Kuitenkaan tämä tutkimus ei sisällä tarkkaa selostusta koodista eikä suoranaista laskentaa, vaan takaa enemmin todisteet siitä että standardin mukaiset menetelmät toimivat magneettilaakeri systeemin todentamisessa.

ACKNOWLEDGEMENTS

This thesis was carried out at the Machine Dynamics Laboratory, at the Department of Mechanical Engineering, Lappeenranta University of Technology. The actual research is part of the Tekes funded HS-EDEN high speed development project that is being conducted at Lappeenranta University of Technology

I would like to express my gratitude to my examiners and supervisors Professor Jussi Sopanen and Docent Harri Eskelinen. You have withstood my infernal amount of questions about related and unrelated matters to this subject.

Secondly I want to thank my supervisor Janne Heikkinen, M.Sc., for providing specific information about the project and for giving forceful feedback during this study. In addition I want to thank Alexander Smirnov, Dr.Tech, for giving me information about the stability margins and AMB control systems.

I am also very grateful to my father Jorma Hakonen and of course the rest of my family who have supported me through my whole educational career with mental and financial support. Without you this wouldn't have been possible. I also want to give credit to one special friend of mine, who has helped me with the language and spelling issues in this thesis. Then my dear diving friends from Lappeenranta have helped me to take thoughts away from the subject.

Finally I want to thank all my friends from Lappeenranta. My time here is running out and I am going to miss you all. Wish you all only the very best.

Lappeenranta, November 8th, 2014

Ville Hakonen

TABLE OF CONTENTS

1 Introduction 10
1.1 Research background 11
1.2 Objectives and limitations of the study 12
1.3 Structure of the study 13
2 The working principle of an Active Magnetic Bearing System 15
2.1 Structure of the AMB system 15
2.2 Rotordynamic 18
2.2.1 Rigid rotor model 19
2.2.2 Flexible rotor model 21
2.3 Electrical actuators 24
2.3.1 Electromagnets 24
2.3.2 Power amplifiers 28
2.4 Control system 29
2.4.1 Classical control 30
2.4.2 Modern control 32
3 API and ISO standard for AMB system 36
3.1 ISO 14839 standard 36
3.1.1 AMB systems mechanical sizing instructions 37
3.1.2 Vibration analysis and test 38
3.1.3 Stability margin 40
3.1.4 Unbalance control 43
3.1.5 Touchdown test 46
3.2 API 617 standard 48
3.2.1 System designing 49

3.2.2 AMB system's performance test in shop and field conditions 51
3.3 Discussion regarding the API and ISO standard 52
4 Verification of the AMB system under design 54
4.1 Introducing the system 54
4.2 The standardized design specifications list and material specifications 58
4.3 Simulation 60
4.3.1 Vibration and unbalance response analysis 60
4.3.2 Stability margin analysis 62
4.3.3 Touchdown test 66
5 Results 72
5.1 Key results 72
5.1.1 New information produced 72
5.2 Side results 73
6 Discussion 74
6.1 Objectivity of research 74
6.2 Reliability analysis 75
6.3 Value and Applications to new results 76
6.4 Follow-up research 76
7 Summary and conclusions 77
References 79
Appendix 83
APPENDIX I: Typical radial magnetic bearing sizing chart.
APPENDIX II: Typical thrust magnetic bearing sizing chart.
APPENDIX III: Design specification check list.
APPENDIX IV: Touchdown bearing clearance.
APPENDIX V: Touchdown test rotor orbit responses.

LIST OF SYMBOLS AND ABBREVITATIONS

Roman letters

A	System matrix	
B	System matrix	
B	Magnetic flux density	T
B_{fe}	Magnetic flux density of steel	T
B_s	Saturated magnetic flux density	T
C	System matrix	
$C_{\min}$	Minimum radial/axial clearance	µm
D	System matrix	
$D_{\max}$	Maximum displacement peak	µm
$\mathbf{D}_{\mathrm{m}}$	Damping matrix	
E	Outside excitation signal	
e	Position error signal	
F_{+}	Force of the upper electromagnet	N
F_{-}	Force of the lower electromagnet	N
$\boldsymbol{F}$	Force vector	N
F	Force	N
f	Frequency	Hz
f_0	Base frequency	Hz
G_0	Open loop transfer function	
$\mathbf{G}_{\mathrm{M}}$	Gyroscopic matrix	
G_s	Sensitivity function	
g	Gravity, $g = 9.81\ {}^{m}/_{s^2}$	m/s^2
H	Magnetic field	A/m
I_{synch}	Synchronous bearing current	A
i	Current	A
$\boldsymbol{i_c}$	Control current vector	A
$\mathbf{i_b}$	Bias current	A
K	Stiffness matrix	
K_f	Kalman filter factor	
K_d	Derivate part factor of PID	

K_i	Integrate part factor of PID	
K_p	Proportional part factor of PID	
$\mathbf{K_r}$	Constant matrix	
k	Stiffness	
k_i	Current-stiffness factor	N/A
k_s	Position-stiffness factor	N/m
l_{fe}	Length of the magnetic path	m
$\mathbf{M}$	Mass matrix	kg
m	Mass	kg
$\mathbf{N}$	Shape function matrix	
$\mathrm{N_c}$	Number of coil windings	
N_p	Number of magnetic pole pairs	
P	Number of nodes used in FEM analysis	
$\boldsymbol{p}$	Modal coordinate	
$\boldsymbol{q}$	Generalized displacement vector	m
$\boldsymbol{q}_i$	Vector of states	
s	Laplace variable	
s	Air gap	m
$\mathbf{T1}$	Transformation matrix	
$\mathbf{T2}$	Transformation matrix	
$\mathbf{T}_{\mathrm{s}}$	Rotating sensor coordinate system matrix	
$\mathbf{T}_1$	Magnetic bearing coordinate system matrix	
t	Time	s
U_{p}	Supply voltage	V
V_1	Response signal one	
V_2	Response signal two	
V_{a}	Volume of air gap	m^3
$\mathbf{W}$	Constant power spectral density matrix	
W_a	Field energy in air gap	Ws

Greek letters

α	Angle at which the magnetic force influences the rotor	O
β	Tilting motion	
Φ	Magnetic flux	Wb
$\boldsymbol{\phi_r}$	Mode matrix	
μ_m	Desired output voltage	V
μ_0	Permeability of vacuum, $\mu_0 = 4\pi * 10^{-7}$	Vs/Am
μ_r	Permeability of ferromagnet	Vs/Am
τ	Time constant	s
Ω	Rotor rotational speed	rad/s
ω	Eigen value	
ω_d	Process noise	dB
ω_n	Measurement noise	dB
$\boldsymbol{\varphi}$	Eigen vector	
ζ	Damping ratio	

Abbreviations

AMB	Active Magnetic Bearing
API	American Petroleum Institute
DOF	Degree 0f Freedom
FFT	Fast Fourier Transform
FEM	Finite Element Model
ISO	International Organization for Standardization
PID	Proportional, Integer and Derivate
LQR	Linear Quadratic Regulator
LQG	Linear Quadratic Gaussian
MIMO	Multi Input – Multi Output
ODC	Optimum Damping Control
SISO	Single Input – Single Output
UFCC	Unbalance Force Counteracting Control
UFRC	Unbalance Force Rejection Control
RoBeDyn	Rotor-Bearing Dynamics

1 INTRODUCTION

The idea of a levitating mechanical structure is not a new idea. First, it was introduced and decided in 1842 by a scientist called Samuel Earnshaw, but considered impossible. However, the idea was developed over several decades, and in 1937 Kemper applied for a patent for hovering suspension. This invention had many applications, for example the MAGLEV elevated guide way for railways. However, the first rotating magnetic bearings were introduced in 1976 by a company called S2M. In Figure 1 is shown modern version of rotating Active Magnetic Bearing system. Which also are the main studied structure. (Schweitzer. 2009, p. 7)

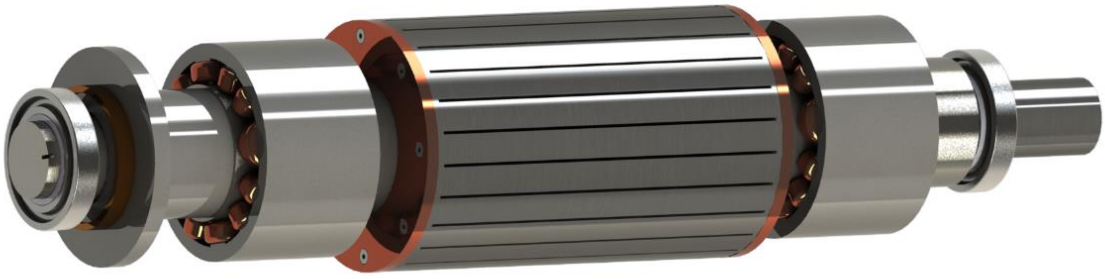

Figure 1. Studied Active Magnetic Bearing system, where is shown both radial AMB stators, axial AMB disk, both touchdown bearings and rotor.

This introductory section of this study is divided into three different parts. The first part of this introduction contains a brief overview of Active Magnetic Bearing (AMB) systems, the benefits and disadvantages of using AMBs and information about the HS-EDEN project.

The second part deals with the objectives and limitations of the study, where the different goals are handled separately. In this section, the important part is also the study limitations. Although given the amount of limitations, some this information is assumed to be known by the reader. The final part of this introduction contains information regarding of the structure of this study.

1.1 Research background

As mentioned above, the idea of a levitating mechanical structure is long-standing, the number of applications and research projects dealing with Active Magnetic Bearings (AMB) have risen in the last few decades because the industry has been demanding more high speed technology applications. The AMB systems are a suitable solution to industries with the demands of large medium- and high-speed machinery. (Hynynen. 2011. p. 18). The advantage of using AMB is the almost non-existent friction and because they do not necessarily require any lubrication. They are quiet to operate and they have adjustable stiffness and damping unlike the traditional fluid film bearings. Overall, these things offer almost unlimited control of the AMB and makes them superior to the classic bearing system. (Schweitzer. 2009, p. 15-16)

AMB applications are used for example in:

- Machining, grinding, high-speed- and high-precision milling provides application to AMB system in manufacturing industry.
- Turbo machinery, for example natural gas production, gas turbines, underwater high durability compressors etc. This is the main application area of the AMB system.
- Energy production and storage in flywheels and plant generators.
- Medical industry uses AMB systems in artificial heart pumps.
- Vacuum and cleanroom systems. AMB systems are used in turbo molecular vacuum pumps in the semiconductor industry providing the high vacuum needed for the chip manufacturing.

Despite all the applications, advantages and disadvantages of the AMB systems are the high cost for the investor. The low standardization level, designing needs knowledge of several engineering fields (mechanical, electronic, control and software) and the size of the AMB, which is larger than traditional oil film bearing. (Schweitzer, 2009, p. 16) (Swanson, et. al., 2008, p. 134)

Lappeenranta University of Technology (LUT) has researched high-speed technology for the past 30 years and the AMB systems for more than 10 years. The HS-EDEN project was formed in 2013 with the great ambition to develop AMB systems for more commercial use. This means that the reliability needs of the technology needed to be improved, because when the new machinery is put in use, it needs to prove that it is more reliable and economical than the traditional bearing systems. The HS-EDEN project is aimed to end in May 2015. (LUT-news, 2013)

1.2 Objectives and limitations of the study

The goal of this master's thesis is to provide information about AMB designing and system verification by referencing the International Standards Organization (ISO) and the American Petroleum Institute (API) standard information and instructions. Standardized information will be the guideline to making the verification simulation tests for system under design. These standards will also provide a guideline for the new designer in verification process. Designing of new models are a small part of this thesis, but it is important to edit models by using the design guidelines and design specification check list information from ISO 14839-4 standard, because the simulation tests are based on that information. This collected data is always placed next to the simulation models and therefore the data can easily be found and this makes the ideal simulation test results possible.

Simulation based tests are divided into three individual tests, the first test is vibration analysis, where the goal is to find the vibration zone group from the test system. Vibration analysis can be used to evaluate and categorize different machinery. This test also includes unbalance response analysis which is more similar to a theory analysis than a testing method. In this test, the goal is to a find proper unbalance control system and make the verifying simulation run to see that the unbalance control is working correctly. The second test evaluates the stability margin of the system and it is based on a similar kind of methods as the first one. This is the so called zone evaluating method, and it is effective when determining the systems stability group and therefore to obtain the system's suitable operating purposes. The third and final simulation is based on the touchdown bearings and touchdown test where the goal is to find what kind of orbit responses the rotor performs when it is dropped from its levitation position.

This study concentrate on AMB testing and verification methods given by the ISO standard. Therefore calculation is limited to theory section and explaining the Matlab simulation codes are not included in this study. In the theory section, only the very basic information about the AMB systems is introduced, however chapter three gives more information about the standardized test methods. Chapter three is dealing mostly with the ISO 14839 standard because it gives more specific information about the systems and naturally because this research is conducted in Europe and the ISO is European organization so it is more suitable to deal with it than with the API.

1.3 Structure of the study

This thesis is divided into seven different chapters, all of which deal with different subjects. These subjects are the introduction, the theoretical introduction to the AMB systems, the theory dealing with ISO and API standard, the practical part of the ISO standard, analyzing the results, discussion and finally a summary of the whole study.

Chapters one and seven are the introduction and summary. Where, the introduction contains the basic information and structures of the study. And the summary summarizes the whole thesis to the short chapter where are all the important information and the key results are presented in a simplified way.

Chapter two and three are the more theoretical part of the thesis. Chapter two gives the basic information and abstracts that are required to understand the main idea of the chapter three. Chapter three is the main theory part and introduces the different verification methods and gives the designing instructions that are determined in the ISO and API standardizations.

The main purpose of chapter four is to collect the data from the series of simulation tests that have been performed by using the Matlab R2013b Rotor-Bearing Dynamic (RoBeDyn) program in which the numerical simulation can be done precisely and efficiently. Chapter three contains also the practical part of the product data management by collecting all the important designing data into one table which can easily be used to follow the design models created by using the SolidWorks 2013 3D-modelling program.

The fifth chapter contains, the explanation regarding the important and new main results and their possible applications. Moreover, in this chapter the possible side results are introduced, which often arise during the simulation research. However, although chapter five deals with the results it is chapter six, the discussion, which is the main empirical part of this thesis and contains the reliability analysis and discusses the value of the new results and the possible applications. The final part of chapter six deals with possible future research and discusses what might be the best approach.

2 THE WORKING PRINCIPLE OF AN ACTIVE MAGNETIC BEARING SYSTEM

The basic working principle of the AMB system can be divided into four main areas, the AMB system structure and components, the system dynamics, the electrical actuators and an introduction to the control design. The mechanical structure provides an example of what kind of components there are and where they are usually found in the AMB system. Mechanical modeling continues on to the rotor dynamics where the rotor designing can be divided into rigid and flexible rotor models. The electrical design is the next part and is limited to the electromagnets with magnetic force analysis and power amplifiers. The final part of this chapter contains basic information about the control systems that are used in AMB systems.

2.1 Structure of the AMB system

The Active Magnetic Bearing system is a good example of a mechatronic machine because the AMB system can be divided into three parts. The mechanical part are the shaft and the retainer bearing units and case. The electrical parts are the sensors, amplifiers, electromagnets and electrical circuit. Finally, the control system contains the microprocessors and programs. These basic AMB components are shown in Figure 2. (Schweitzer, 2009, p. 4-5).

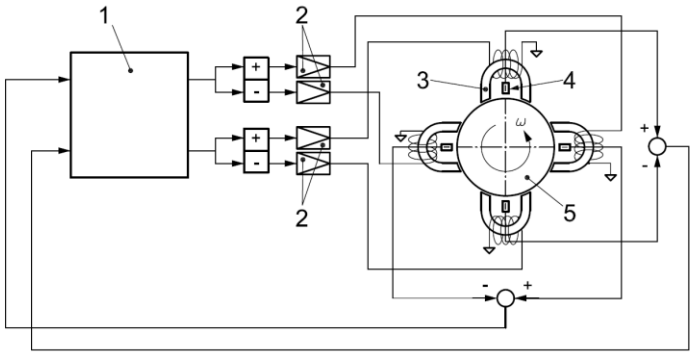

Figure 2. Schematic of the functions principle of the AMB. Number 1 is the controller box, 2 is the power amplifiers, 3 is the magnetic coil, 4 is the displacement sensor and 5 is the rotor with angular frequency. (ISO 14839-4, 2013, p. 2)

Considering the system, the rotor of the AMB system is in the center of the magnetic flux, which is created by the surrounding electromagnets. A typical illustrative cross section of the radial actuator is shown in Figure 3. The magnets form two pairs, and the angle between the magnets is 45 degrees to the global gravity axis. In total there are 8 magnetic poles. This allows the actuator to pull the shaft in any radial direction. However, in Figure 4, the commercial arrangement of AMB is shown where the four different sections remain but the magnet is divided into four different quadrants by interconnecting the coils within each quadrant. (Swanson, et. al. 2008, p. 134)

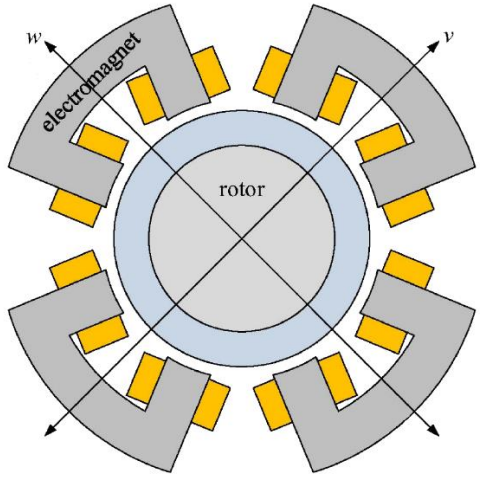

Figure 3. Illustrative cross section of AMB magnets. (Swanson, et. al. 2008, p. 134)

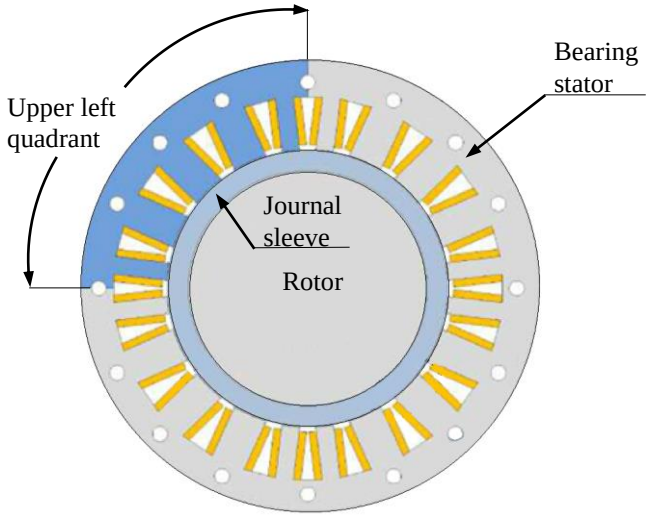

Figure 4. A commercial radial AMB. One quadrant is shown in a blue color. (Swanson, et. al. 2008, p. 135)

Typically, the AMB system contains two units of radial magnetic bearing stator assemblies, Figure 5, which provides the rotating possibility to the rotor, similar to traditional bearings. These will keep the rotor in the center of the bearing sets with the help of the control system which reads the signals from the radial displacement sensors to provide adjustment possibilities by changing the control current I_c. (API 617- 4, 2002, p. 41)

The radial bearing units cannot take any of the axial force. That is why AMB systems usually have one pair of axial magnetic bearing stator assemblies, which are shown in Figure 5. Axial magnetic bearing sets work just like the radial bearings but they resist only axial forces and none of the radial forces. (ISO 14839-1, 2992, p. 4 - 5)

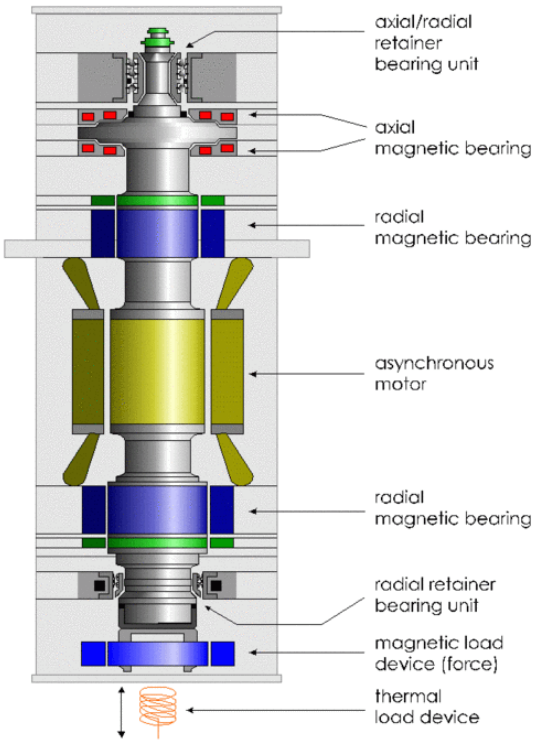

Figure 5. AMB system structure. Main components are shown in the figure. (Hochschule Zittau/Görlitz, 2014)

Axial and radial bearing sets provide stationary levitation and full position control to the rotor but as shown in Figure 5 the AMB system is often powered by an asynchronous motor because it does not need mechanical commutation, thus providing power with good efficiency, and offers a reliable solution to long term operation machinery. (Pyrhönen et. al., 2008, p. 131)

In Figures 5 and 6, the retainer bearing or touchdown bearing units are presented. These bearings are in the system in case of magnet or system malfunction when the rotor drops from a neutral position on the backup bearings, and they will reduce possible breakdowns. However, the main application to these retainer bearings are to fully function machinery, the rotating support to the AMBs during the acceleration phase of the rotor and when machinery is not running the retainer bearings provides support to the rotor that it does not lay on the AMBs. (ISO 14839-4, 2012, p. 18)

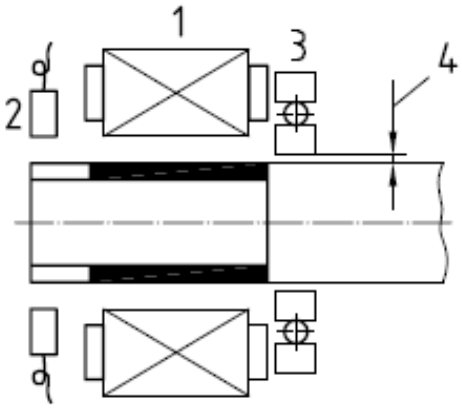

Figure 6. Auxiliary bearing principle, where 1 = AMB, 2 = Displacement sensor, 3 = Retainer bearing, 4 = Retainer bearing air gap (ISO 14839-2, 2004, p. 2)

2.2 Rotordynamic

Rotordynamics are an essential part of designing in the AMB system. Typically, rotordynamics are divided in two main rotor models. A rigid rotor model where all flexible eigenfrequencies are beyond the bandwidth of the control system and the maximum rotational speed of the system. A flexible rotor model where the rotor have been designed thin and these typically have flexible eigenfrequencies in a low low frequency range where they can be affected by control and/or are passed during run-up and run-down. Flexible rotors require more detailed modeling because of their elastic behavior. (Lösch, 2002, p. 15)

Equation (1) presents a general description of the AMB system dynamics, which can be structured into different forms between a rigid and a flexible rotor model. This equation is based on Newton's second law and it also includes a coupling between different inputs and outputs. More specific theory behind this equation can be found from Genta's Dynamic of Rotating systems (Genta, 2005)

$$\mathbf{M}\ddot{\boldsymbol{q}}(t) + (\mathbf{D}_M + \Omega \boldsymbol{G}_M)\dot{\boldsymbol{q}} + \mathbf{K}_q = \boldsymbol{F}(t) \quad (1)$$

where **M** is the mass matrix, $\mathbf{D}_\mathrm{M}$ is the damping matrix, $\mathbf{G}_\mathrm{M}$ is the gyroscopic matrix, Ω is the rotor rotational speed, **K** is the stiffness matrix, $\boldsymbol{F}$ is the force vector and $\boldsymbol{q}$ is the generalized displacement vector. (Smirnov, 2012, p. 34)

2.2.1 Rigid rotor model

A system containing a rigid rotor model, two radial AMB and a gyroscopic effect are considered when modeling the AMB rigid rotor model which is shown in Figure 7. The displacement vector $\boldsymbol{q} = [x\ y\ \theta_x\ \theta_y]^\mathrm{T}$ describes the motion of a rotor with respect to the center of mass. The displacement of body is shown by *x* and *y*, rotations around y axis is θ_y and around *x* axis is θ_x. There are altogether four degrees-of-freedom (DOF) because the fifth and sixth DOFs are motions along and around the *z* axis and they are special cases, which means that these motions along the *z* axis is treated separately with an axial bearing. Using these information Equation (1) can be changed to represent the rigid rotors mass center, (Chen, 2005, p. 119-124)

$$\mathbf{M}\ddot{\boldsymbol{q}} + \Omega\mathbf{G}_\mathrm{M}\dot{\boldsymbol{q}} = \boldsymbol{F}, \quad (2)$$

where the matrix components are constructed as

$$\mathbf{M} = \begin{bmatrix} m & 0 & 0 & 0 \\ 0 & m & 0 & 0 \\ 0 & 0 & I_y & 0 \\ 0 & 0 & 0 & I_x \end{bmatrix} \quad \mathbf{G}_\mathrm{M} = \begin{bmatrix} 0 & 0 & 0 & 0 \\ 0 & 0 & 0 & 0 \\ 0 & 0 & 0 & I_z \\ 0 & 0 & -I_z & 0 \end{bmatrix} \quad \boldsymbol{F} = \begin{bmatrix} f_x \\ f_y \\ \theta_x \\ \theta_y \end{bmatrix} \quad (3)$$

Where the mass matrix **M** shows the mass of the rotor m and the transversal moments of inertia I_x and I_y. Gyroscopic matrix $\mathbf{G}_\mathrm{M}$ shows the rotational inertia I_z around the *z* axis, respectively. Forces affected by the *x* and *y* axis directions are f_x and f_y. Finally θ_x and θ_y are the moments that affect the same axes. Figure 7 shows the coordinate systems of the rigid rotor disk. (Yoon, et. al., 2013, p. 29-31)

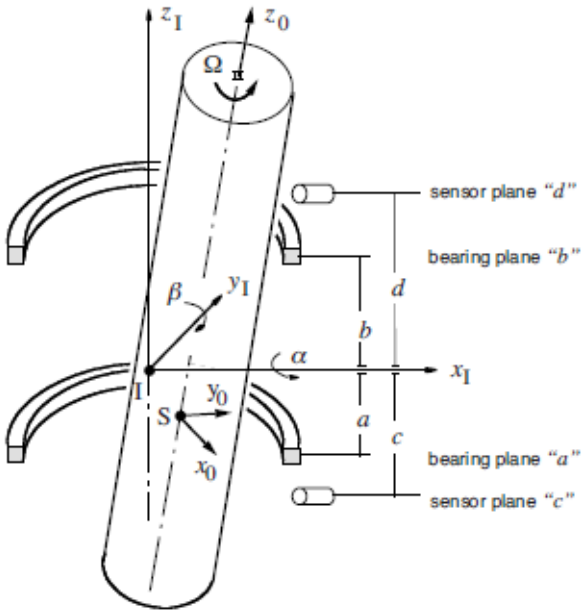

Figure 7. Coordinate systems in a rigid rotor disk. (Schweitzer, 2009, p. 172)

By using the rotor coordinates, Equation (2) can be written as

$$\mathbf{M_b}\ddot{\boldsymbol{q}}_b + \Omega\mathbf{G_b}\dot{\boldsymbol{q}}_b = \mathbf{K_s}\boldsymbol{q}_b + \mathbf{K_i}\boldsymbol{i}_c, \tag{4}$$

where $\mathbf{K_s}$ is the position stiffness matrix, and $\mathbf{K_i}$ is the current stiffness matrix. The index b represents the coordinates of the bearing in the displacement vector $\boldsymbol{q}_b = [x_A\ y_A\ x_B\ y_B]$, which notes the rotor displacement in bearing *A* and bearing *B* along *x* and *y* axis. $\boldsymbol{i}_c$ is a control current vector, $\boldsymbol{i_c} = \left[i_{c,x,A}\ i_{c,y,A}\ i_{c,x,B}\ i_{c,y,B}\right]$, which indicates the current of electromagnets at bearings *A* and *B* in the *x* and *y* axis directions. Finally the transformation from global coordinates to bearing coordinates can be now done:

$$\boldsymbol{q}_b = \mathbf{T_i}\boldsymbol{q} \tag{5}$$

$$\mathbf{G_b} = \mathbf{T_2^T}\mathbf{G_M}\mathbf{T_2} \tag{6}$$

$$\mathbf{T_2} = \mathbf{T_1}^{-1} \tag{7}$$

$$\boldsymbol{q_s} = \mathbf{T_s}\boldsymbol{q}, \tag{8}$$

where $\mathbf{T_s}$ shows the rotating sensor coordinate system. Transformation matrices can be written as

$$\mathbf{T}_1 = \begin{bmatrix} 1 & 0 & 1 & 0 \\ 0 & 1 & 0 & 1 \\ 0 & -a & 0 & b \\ -a & 0 & b & 0 \end{bmatrix} \quad \mathbf{T}_s = \begin{bmatrix} 1 & 0 & 1 & 0 \\ 0 & 1 & 0 & 1 \\ 0 & -c & 0 & d \\ -c & 0 & d & 0 \end{bmatrix} \tag{9}$$

where a and b is in $\mathbf{T}_1$ the distance from center of the rotor to the specific bearing. Unlike, in $\mathbf{T}_s$ c and d is the distance to the specific sensors from center of the rotor. (Schweitzer, 2009, p. 173-175)

2.2.2 Flexible rotor model

Modeling the rotor by using a flexible rotor model is more realistic than modeling with rigid models because every rotor is flexible. Usually, the flexible rotor model uses finite element modelling methods (FEM) where the model is divided into a finite number of similar elements depending on the geometry of the rotor, application and the operating speed. Typically, in rotordynamics these elements are cut in the cylindrical beam elements that are connected together with nodes. A good method of modelling a flexible rotor is the Timoshenko's beam element theory, Figure 8. The benefits of using this beam element method in FEM modeling are that it takes into account both deformation and shear force. In this theory, the beam has two nodes at both ends of the beam and 6 DOFs per each node. Figure 8 shows the coordinate system of the beam. (Genta, 2005, p. 156 – 159).

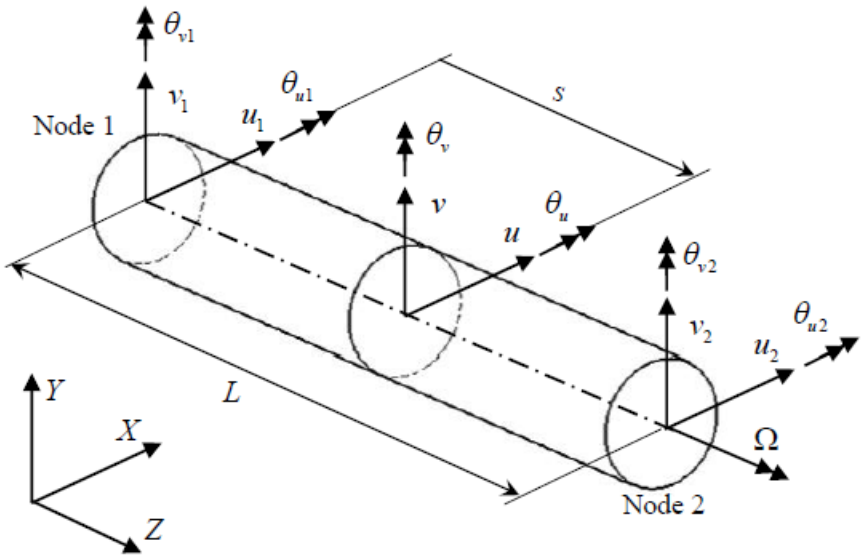

Figure 8. The coordinate system of the single beam element (Kärkkäinen, 2007, p. 23)

Using a general equation of motion (Equation (1)) and the information from Timoshenko's beam theory each single element can be described by

$$\mathbf{M}_{\mathrm{m}}\ddot{\boldsymbol{q}}_m + (\mathbf{D}_{\mathrm{m}} + \Omega\mathbf{G}_{\boldsymbol{m}})\dot{\boldsymbol{q}}_m + \mathbf{K}_{\mathrm{m}}\boldsymbol{q}_{\boldsymbol{m}} = \boldsymbol{F}_m, \tag{10}$$

where the component matrices are already opened in section 2.2.1, the rigid rotor model and $\boldsymbol{q}_m = \left[x_m\ y_m\ \beta_{x,m}\ \beta_{y,m}\right]^T$ are the vector of states. The bottom indicator *m* indicates the number of the elements *m* = 1, 2, 3…, *n*. Now the final shape of the rotor can be described by **N** which is a shape function matrix (Kärkkäinen, 2007, p. 25)

$$\boldsymbol{q}_i^e = \mathbf{N}(s)\boldsymbol{q}_i = \begin{bmatrix}\mathbf{N}_{\mathrm{T}}(\mathrm{s}) \\ \mathbf{N}_{\mathrm{R}}(\mathrm{s})\end{bmatrix} q^e, \tag{11}$$

and after amending the general motion equation becomes

$$\mathbf{M}^{\mathbf{e}}\ddot{\boldsymbol{q}}^e + (\mathbf{D}^{\mathbf{e}} + \Omega\mathbf{G}^{\mathbf{e}})\dot{\boldsymbol{q}}^e + \mathbf{K}\boldsymbol{q}^e = \boldsymbol{F}^e \tag{12}$$

In Equation (12) there are a huge number of state variables because they come from the number of finite elements used in the model multiplied by the number of DOFs in connection node. This makes the calculation processing long and challenging when using a traditional time integration solver scheme. The method of solving this calculation is called a component mode synthesis where the deformations of the rotor are assumed to be linear. This assumption gives a possibility of using modal coordinates instead of nodal coordinates when determining rotor's deformation. Moreover, the benefits of using modal coordinates are that the number of deformation variables are reduced and the calculation process will lead to diagonal matrices in the description of mass, stiffness and damping matrices. (Khulief, 1997, p. 47)

The component mode synthesis requires calculating the vibrating modes from the following eigenvalue problem. However this is not the only way to calculate eigenvectors. In some applications using static correction modes can lead to more accurate results. (Kärkkäinen, 2007, p. 32)

$$[\mathbf{K} - \boldsymbol{\omega}_k{}^2\mathbf{M}]\boldsymbol{\varphi}_k = 0 \tag{13}$$

where ω_k is the k[th] eigenvalue and $\boldsymbol{\varphi_k}$ is the k[th] eigenvector. After solving the Equation (13), the results are where the number of modes of the rotor is exactly the same than number of degrees of freedom. In addition, only the low frequency modes contribute significantly to the response of the system. High frequencies complicate the time integration procedure. Therefore, high frequency modes can be ignored without loss of accuracy. (Khulief, 1997, p. 47-50)

Currently only the selected vibrations are in use. Where a mode matrix $\boldsymbol{\phi}_\mathbf{r}$ with *n* selected modes are in the form of Equation (14) (Kärkkäinen, 2007, p. 32)

$$\boldsymbol{\phi}_r = [\varphi_1 \ \ldots \ \varphi_n] \tag{14}$$

Selecting the modes can be used to help the strain energy or just visual appearance of the mode matrix. In the selection process are one or two points where attention has to be paid, e.g. the total number of modes and particularly the capabilities of the modes that describe the behavior of the system.

A non-reduced mode matrix $\boldsymbol{\phi}$ can be used when forming the coordinate transformation that relates the exact physical coordinate's $\boldsymbol{q}$ to the modal coordinate's $\boldsymbol{p}$, (Kärkkäinen, 2007, p. 32)

$$\boldsymbol{q} = \boldsymbol{\phi}\boldsymbol{p} \tag{15}$$

Using the Equation (15) as a basis, the physical coordinates can be estimated using the reduced mode matrix and corresponding modal coordinates $\boldsymbol{p}_r$, (Kärkkäinen, 2007, p. 32)

$$\boldsymbol{q} \approx \boldsymbol{\phi}_\mathbf{r}\boldsymbol{p}_r \tag{16}$$

As a result of the mode synthesis process the motion equation can be written in its final form by using modal coordinates (Kärkkäinen, 2007, p. 33)

$$\boldsymbol{\phi}_{\mathrm{r}}^{\mathrm{T}}\mathbf{M}\boldsymbol{\phi}_{\mathrm{r}}\ddot{\boldsymbol{p}}_r + (\boldsymbol{\phi}_{\mathrm{r}}^{\mathrm{T}}\mathbf{C}\boldsymbol{\phi}_{\mathrm{r}} + \Omega\boldsymbol{\phi}_{\mathrm{r}}^{\mathrm{T}}\mathbf{G}\boldsymbol{\phi}_{\mathrm{r}})\dot{\boldsymbol{p}}_r + \left(\boldsymbol{\phi}_{\mathrm{r}}^{\mathrm{T}}\mathbf{K}\boldsymbol{\phi}_{\mathrm{r}} + \frac{1}{2}\dot{\Omega}\boldsymbol{\phi}_{\mathrm{r}}^{\mathrm{T}}\mathbf{G}\boldsymbol{\phi}_{\mathrm{r}}\right)\boldsymbol{p}_r = \boldsymbol{\phi}_{\mathrm{r}}^{\mathrm{T}}\boldsymbol{F}_{tot} \tag{17}$$

where $\boldsymbol{F}_{tot}$ is a vector of the sum of the externally applied forces. Mode synthesis can be complex in the application where physical forces are transformed into modal forces or the modal coordinates are transformed into physical coordinates. However, the AMB system are exceptions because of the small bearing forces and the few sensor displacements that are needed during the solution of the equations of motion. (Kärkkäinen, 2007, p. 33)

2.3 Electrical actuators

As mentioned above, the AMB system is a mechatronic machine and the levitating movement is based on magnetic force generated by electromagnetic flux. This force can be calculated and it can be used for the designing problems in the AMB system.

Amplifiers are an important part of AMB system's electrical circuits. The main application of the power amplifiers is to deal with the followings problems:.

- Energy losses in the switching amplifier itself
- Energy losses in the copper wiring
- Losses in stator and rotor caused by Eddy current and hysteresis

With proper amplifier design these problems can be avoided and the system will be reliable.

2.3.1 Electromagnets

Magnetic bearings can be approximated with the U-shape magnet core as in Figure 9, where the coil's current *i* generates a magnetic field *H* in the ferromagnetic core according to Ampere's law. (Yoon, et. al., 2013, p. 58)

$$\oint H \cdot dl = N_c i. \tag{18}$$

where N_c is the number of coil windings and l is the length of the magnetic coil. If the magnet is ferromagnetic, the magnetic field is H_{fe} and the air gap is H_a. From Figure 9 the length of the magnetic path can be calculated from $l_{fe} + 2s$, where l_{fe} is the total length of the magnetic path and s is the air gap between magnet and rotor. Now Ampere's law can be restructured,

$$l_{fe}H_{fe} + 2sH_a = N_c i. \tag{19}$$

The magnetic flux density B is

$$B = \mu_o \mu_r H, \tag{20}$$

where the magnetic permeability constants for air $\mu_r \sim 1$ and for vacuum $\mu_o = 4\pi \cdot 10^{-7}$ (Valtanen, 2010). This assumes that the magnetic flux Φ is ideal and flows in the core without leakage flux, and the cores cross section A_{fe} is constant in the whole magnetic loop and is the same as the cross area of the air gap A_a. (Yoon, et. al., 2013, p. 60)

$$\Phi = B_{fe}A_{fe} = B_a A_a \tag{21}$$

$$A_{fe} = A_a \tag{22}$$

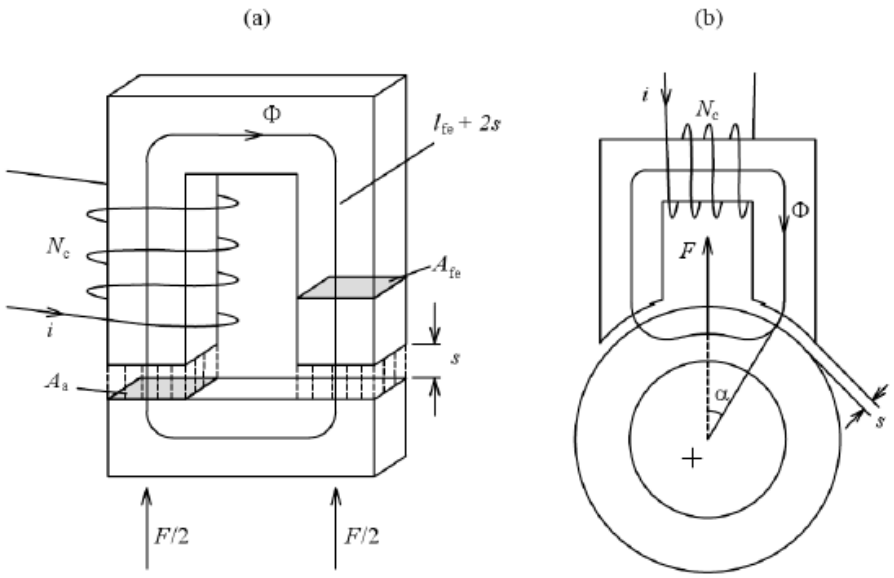

Figure 9. Figure of the AMB (a) U-shaped magnet. (b) Geometry of one pole pair of radial magnetic bearing with four pole pairs. (Schweitzer, 2009, p. 78)

Assuming that the flux density is constant in the core and the air gap,

$$B_{fe} = B_a = B \tag{23}$$

From above the total flux density can be solved and because the permeability of the ferromagnet is $\mu_{fe} >> 1$ the final flux density is, (Yoon, et. al., 2013, p. 59)

$$B = \mu_0 \frac{N_c i}{2s}. \tag{24}$$

Using the information that the force of the magnetic field is generated from the field energy W_a which is stored in the air gap (Schweitzer, 2009, p. 77)

$$W_a = \frac{1}{2} B_a H_a V_a = \frac{1}{2} B_a H_a A_a (2s), \tag{25}$$

where the volume of air gap is V_a. Now the magnetic force is partially derivative from the field energy (Schweitzer, 2009, p. 78)

$$F = \frac{dW_a}{ds} = B_a H_a A_a. \tag{26}$$

Now by substituting, the magnetic force is

$$F = \mu_0 A_a \frac{(N_c i)^2}{(2s)^2} = \frac{1}{4} \mu_0 {N_c}^2 A_a \frac{i^2}{s^2} = k \frac{i^2}{s^2}, \tag{27}$$

where the stiffness k is

$$k = \frac{1}{4} \mu_0 {N_c}^2 A_a \tag{28}$$

Usually the magnetic force affects at an angle α like in Figure 9 (b), for example, the eight-pole bearings, $\alpha = 22.5^{o}$. Therefore, the magnetic force equation changes (Schweitzer, 2009, p. 79 - 80)

$$F = \frac{1}{4}\mu_0 {N_c}^2 A_a \frac{i^2}{s^2}\cos(\alpha) = k\frac{i^2}{s^2}\cos(\alpha) \tag{29}$$

In most AMB applications, magnetic bearings have two counteracting magnets operating in the differential driving mode as seen in Figure 10. The current arrives at the upper magnet as the sum of the bias current i_b and the control current i_c, $i_b + i_c$. However, the lower magnet is the difference between, i_b - i_c. This method gives more linearity to the force-current relationship and now the linearized force can be written as a sum of both magnets, as like shown in Figure 10. (Schweitzer, 2009, p. 79)

$$F_X = F_+ - F_- = k\left(\frac{\left(i_b + i_{c,x}\right)^2}{(s_0 - x)^2} - \frac{(i_b - {i_{c,x}}^2}{(s_0 + x)^2}\right)\cos(\alpha) \tag{30}$$

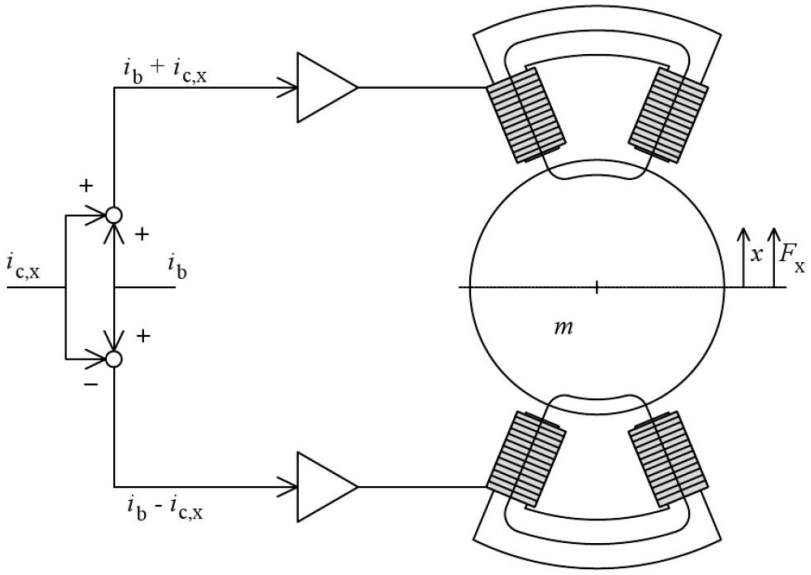

Figure 10. Operation principle of a basic AMB system that operates on the differential driving mode. (Hynynen, 2011, p. 37)

Where F_+ and F_- are the force of the upper and lower magnets, s_0 is the nominal air gap and x is the displacement from the gap in the x-axis direction. By simplifying and linearizing

Equation (30), with the relation $x << s_o$, comes the magnetic force equation (Schweitzer, 2009, p. 79).

$$F_x = \frac{4ki_b}{{s_o}^s}\cos(\alpha)\, i_x + \frac{4ki_b{}^2}{{s_0}^3}\cos(\alpha)\, x = k_i i_x + k_s x, \tag{31}$$

Where the current-stiffness factor k_i and position-stiffness factor k_s, can be defined as

$$k_i = \frac{4ki_b}{{s_0}^2} \tag{32}$$

and

$$k_s = \frac{4ki_b{}^2}{{s_0}^3} \tag{33}$$

Now the final form of magnetic force of an AMB can be defined

$$F_X(x, i) = k_i i_c + k_s x. \tag{34}$$

Despite the fact that Equation (34) is only a linear approximation, practical tests and experience over the years have shown that it works well. However, in special situations like flux saturation, a rotor-stator contact or low bias currents, more complex and nonlinear models are required. (Schweitzer, 2009, p. 77-81)

2.3.2 Power amplifiers

In the AMB system, the power amplifiers converts the control signals to the control currents this is why in industrial applications reliability is one of the most important factors when designing new machinery. Therefore, traditional analog amplifiers have been changing into more modern and reliable switching amplifiers even if they have energy losses. (Schweitzer, 2009, p. 97)

Figure 11 (a) shows the basic working principle of an analog power amplifier. The desired output voltage u_m is generated by driving the primary transistor *T1* with a positive voltage

to the point where voltage u_t over the transistor *T1* is the difference between the supply voltage U_p and the output voltage u_m. Then the conducting transistor have power loss $P = iu_t$ which is only heat. (Schweitzer, 2009, p. 97)

Switching the amplifier, Figure 11 (b), switches the positive and negative voltage among the bearing windings with a given frequency. This pulse-width modulation creates the power loss, $P = u_t i$, in the amplifier considerably lower than in an analog because the voltage u_t runs for just a short period of time through the amplifier. However, the disadvantages of switching the amplifier is that it tends to oscillate, which causes remagnetization loss in the bearing. The oscillation can be changed using a shorter switching period which makes the oscillation weaker. (Schweitzer, 2009, p. 97-98)

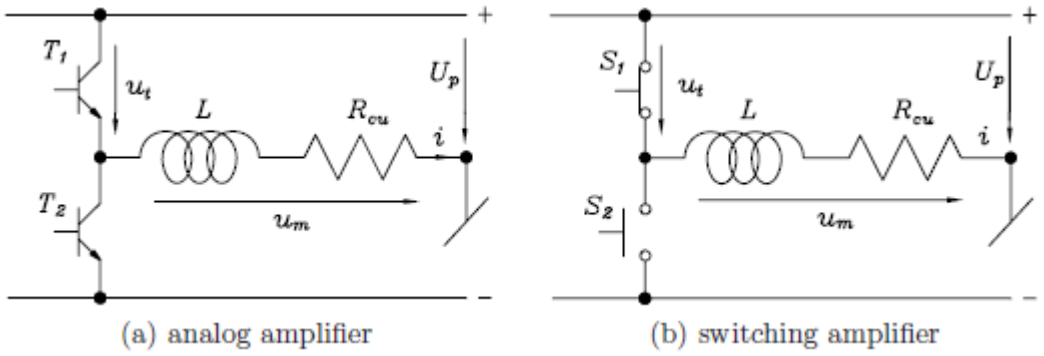

Figure 11. Analog and Switching amplifier principles (Schweitzer, 2009, p. 98)

2.4 Control system

AMB control systems can be divided in two groups, where the classical control system contains a Proportional-Integral-Derivate control (PID) and different variations of this. The PID control systems are simple and universal in many applications and therefore, they can be used for comparison with more complex state-feed-back, model-based controllers. (Jeon, et. al. 2002.). PID controllers are a good method of stabilizing rigid rotor models, but when dealing with flexible rotors the control system becomes complex and difficult to calculate. (Yoon, el. al. 2013, p. 80)

The requirements of the AMB 5 DOFs flexible system are more challenging, therefore, modern control systems are a better choice. Modern control systems are based on two different optimal control laws, Linear Quadratic Regulator (LQR) and Linear Quadratic

Gaussian (LQG), where μ-synthesis and H_∞ control methods are more complex applications. Overall, modern control methods are better for multi-input and multi-output (MIMO) systems because when adding many PID controllers in system calculation process becomes long and difficult. (Yoon, et. al. 2013, p. 81)

2.4.1 Classical control

The classical control system contains the most basic principles of the control system analysis. Usually, these systems are single-input and single-output (SISO) systems and often the system transfer functions are the preferred method for representing dynamic systems in classical control. (Yoon, et. al. 2013. p. 111). Since AMB systems are open loop and unstable, they require a stabilizing controller for their operation. The majority of AMB systems operate with classical PID controllers where a displacement sensor measures the position and displacement of the rotor. After which the position error *e(t)* is computed by comparing the desired and actual rotor position. Based on position error three different components are calculated by the controller:

- The mechanical spring like effect. Force proportional to the error signal ($K_p e$).
- The mechanical damper like effect. Force proportional to the first derivative of the error signal $\left(K_d {de}/{dt}\right)$.
- A component to reduce the steady state error. Force proportional to the integral of the error signal ($K_i \int e\, dt$).

A PID controller can be described as a tunable mechanical mass-spring-damper system where an additional term, added to reduce the rotor position offset due to a DC disturbance. The total force applied on the rotor is the sum of these three force components and it can be generated by, (Yoon, et. al. 2013. p. 75)

$$C_{PID}(s) = K_p + \frac{K_d s}{\tau_d s + 1} + \frac{K_i}{s}. \tag{35}$$

Where τ_d is a small time constant to make the derivate term a proper transfer function.

Classical PID controls have been modified for AMB system purposes only because the AMB system generates lateral dynamics to the rotor and the system levitates. This most common PID application in the AMB system is called Tilt and Translate Control. In this application there are two modes, the parallel, or ‘’translate,’’ mode and the conical, or ‘’tilting’’ mode. These modes are connected in a way that a direct excitation of the translate mode does not affect the tilting mode, and vice versa. The application idea is to use these two rigid modes and stabilize them independently with two separate PID controllers. The layout of the Tilt and Translate control is shown in the Figure 12. (Yoon, et. al. 2013, p. 78)

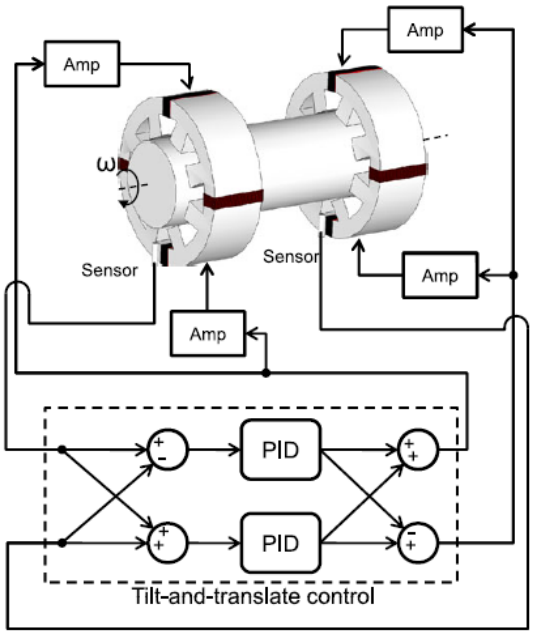

Figure 12. Tilt and translate PID control layout picture. (Yoon, et. al. 2013, p. 79)

Because the PID control system is an SISO based control system, the control output and input signals are combined mathematically and they form the equivalent of a similar transformation of the rotor lateral dynamics. In the ideal case, the system which has transformed will have a decoupled output signal. Afterwards the constructed tilt and translated signals are fed into their independent PID controllers for each rigid mode. The output of the control signal is then reconstruct by two different means depending on the input data. (Yoon, et. al. 2013, p. 78)

- The output from the tilt controller is fed into the bearing actuators with opposite signs to excite the conical mode
- The output from the translate controller is fed into the bearing actuators with equal signs to excite the parallel mode.

This method is mainly used for rigid rotor models and for flexible models this is partially valid because decoupling the signals is a more complex process for higher order modes. However, good decoupling between the tilt and translate channels is mainly obtained in the low frequencies and can be a useful aid during the design process of the PID controllers of the AMB system. (Yoon, et. al. 2013, p. 78-79)

2.4.2 Modern control

Using the optimal control law has one or two advantages over the traditional control systems. By using the modern control system, the energy of the system input and output is minimized. LQR and LQG methods have a chance to achieve better transient response properties for closed-loop systems over the classical optimization methods. This section contains the basic information about LQG and LQR and more specific information about complex μ-synthesis or H_∞ - control systems can be found from Skogestad's Multivariable Feedback control analysis book. (Skogestad, 2005.)

Considering the traditional LQG controller first. Where the state space model is given, the linear time invariant system is included. (Skogestad, 2005, p. 375)

$$\dot{x} = \mathbf{A}x + \mathbf{B}u + \omega_d \tag{36}$$

$$y = \mathbf{C}x + \omega_n, \tag{37}$$

where ω_d is the noise of the process and ω_n is the measurement noise, which usually aims to be an uncorrelated zero-mean Gaussian stochastic process with constant power spectral density matrices **W** and **V**. These matrices can be formed by using ω_d and ω_n information, (Skogestad, 2005, p. 375)

$$E\{\omega_d(t)\omega_d(\tau)^T\} = \mathbf{W}\delta(t-\tau) \tag{38}$$

$$E\{\omega_n(t)\omega_n(\tau)^T\} = \mathbf{V}\delta(t-\tau), \tag{39}$$

and

$$E\{\omega_{\mathrm{d}}(\mathrm{t})\omega_{\mathrm{n}}(\tau)^{\mathrm{T}}\} = 0, \qquad \mathrm{E}\{\omega_{\mathrm{n}}(\mathrm{t})\omega_{\mathrm{d}}(\tau)^{\mathrm{T}}\} = 0, \tag{40}$$

where E is the expectation operator and the term $\delta(t-\tau)$ is a delta function. Now the problem of the LQG control system is to find the optimal value of $u(t)$ that is the value which minimizes the system. Equation (41) is the base of LQG problem, (Skogestad, 2005, p. 375)

$$J_{LQG} = E\left\{\lim_{T\to\infty}\frac{1}{T}\int_0^T [x^T Q x + u^T R u]\,dt\right\}, \tag{41}$$

where Q is the weight on the states formed from positive-semidefinite matrix and R is the weight on the input formed from the positive definite matrix. (Skogestad, 2005, p. 376)

The solution to the LQG problem can be found by using a process known as the Separation Theorem or Certainty Equivalence Principle. These calculation processes are quite simple and the process consists of first determining the optimal control to a deterministic Linear Quadratic Regulator (LGR) problem. Solving the LQR problem is very similar than solving a LQG problem. LQR does not consist of the noise factors ω_d and ω_n when the solution can be written with a simple state feedback law (Skogestad, 2005, p. 376)

$$u(t) = -\mathbf{K_r}x(t), \tag{42}$$

Where $\mathbf{K_r}$ is a constant matrix which is clearly separated from matrices **W** and **V**. The next step is to determine an optimal estimate $\hat{x}$ of the state x, so that $E\{\lfloor x-\hat{x}\rfloor^T\lfloor x-\hat{x}\rfloor\}$ is minimized. The optimal state is given by a filter called a Kalman filter what gives the possibility to find a solution to the LQR problem by replacing x with $\hat{x}$ from Equation (42). (Skogestad, 2005, p. 376)

Now the optimal state feedback of the LQR problem can be determined by using the information that the system is $\dot{x} = Ax + Bu$ with a given non-zero initial state $x(0)$. As in

the LQG problem, in the LQR problem the optimal system needs to find the value to input the signal *u*(t) from Equation (43), (Skogestad, 2005, p. 376)

$$J_{LQR} = \int_0^\infty (x^T(t)Qx(t) + u^T(t)Ru(t))dt. \tag{43}$$

The optimal solution is for any initial state $u(t) = -\mathbf{K_r}x(t)$. Where the $\mathbf{K_r}$ can be determined, (Skogestad, 2005, p. 376)

$$\mathbf{K_r} = \mathbf{R^{-1}B}^T X, \tag{44}$$

As mentioned above, the LQR and LQG process require the Kalman filter. The structure of the Kalman filter is like an ordinary state estimator or observer, as shown in the block diagram in Figure 13. (Skogestad, 2005, p. 377)

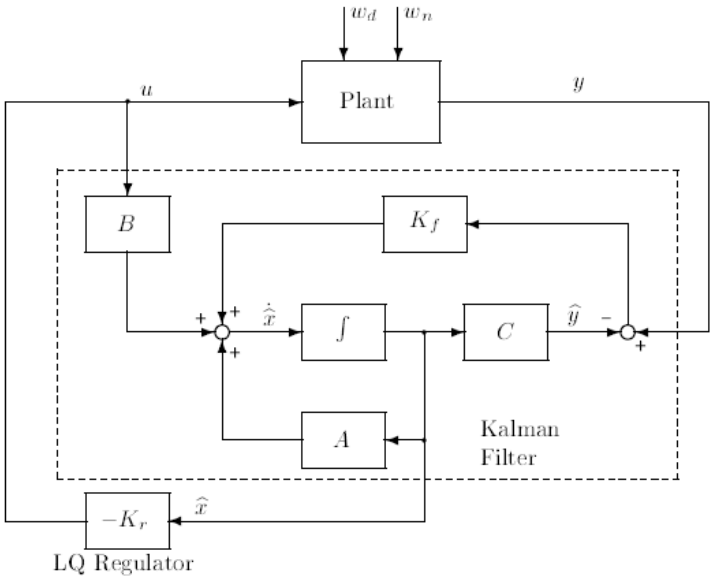

Figure 13. LQG controller with Kalman filter. (Skogestad, 2005, p. 378)

To determine the proper Kalman filter state the estimator needs to be found. This can be seen in Figure 13,

$$\dot{\hat{x}} = A\hat{x} + Bu + K_f(y - C\hat{x}), \tag{45}$$

where the optimal value of K_f is the value that minimizes $E\{[x-\hat{x}]^T[x-\hat{x}]\}$, which is given by

$$K_f = YC^TV^{-1}. \tag{46}$$

Now $Y = Y^T \geq 0$, which is unique positive-semidefinite solution of the algebraic Riccati Equation (47), (Skogestad, 2005, p. 377)

$$YA^T + AY - YC^TV^{-1}CY + W = 0 \tag{47}$$

The purpose of the Kalman filter is to estimate the system's states over time. The filter contains physical model of the plant and constantly updates the model states based on the difference between expected plant output and the actual measurement. It can be said that Kalman filter operates recursively on pulses of input data to produce a more accurate estimate of the underlying system state. (Kalman, 1964 p.51-55)

3 API AND ISO STANDARD FOR AMB SYSTEM

Chapter two contains the basic abstracts and basic models of the AMB system theory that will be required to fully understand the content of this chapter. These basic theories will be applied to the standardization of the AMB system by using the instructions from ISO 14839 standard and API 617 standard. However, the main focus is on the ISO standard because it will determine the design parameters, gives example simulation models and for the regional view is wider than in the API standard. The API standard contains only a shallow information section about AMB systems and it uses mainly imperial units.

3.1 ISO 14839 standard

The ISO 14839 standard has been separated into four different parts. Part 1 contains the basic vocabulary and explains the terms that relate to the machinery equipped with AMB. (ISO 14839-1, 2002, p. 1–2) Part 2 contains the evaluation of the vibration which describes how the shaft vibratory displacement should be measured, and what are the maximum limits of displacement in specific rotating speed zones by using the vibration test. (ISO 14839-2, 2004, p. 1–3). Part 3 contains stability margin analysis and this part has three main goals. First goal is to provide mutual understanding between vendors and user, engineers and electrical engineers about the stability margin. Second goal is to provide an easier development method than before for the stability margin that can be useful in simplifying contract concerns, commission, and system maintenance. Final goal is to collect mutual understanding from the industry about AMB rotor system stability and design. (ISO 14839-3, 2006, p. 1) Finally, part 4 is the technical guideline that gives information about the sizing of the AMB system, gives the information about the design specification check list and examples of the AMB touchdown test and vibration test. Moreover, in part 4 there are good recommendations and information guidelines about the condition monitoring systems, the regular maintenance and inspection procedures. (ISO 14839-4, 2012, p. 1)

In this study the processing of the ISO standard is divided into five different parts. The first part contains the necessary information about the AMB system's mechanical design, which covers the magnetic bearing clearances and touchdown bearing materials as well as different ways to install them. The second part deals with the AMB system vibration and it gives

information regarding how the stability test should be performed. The third part contains the evaluation of the stability margin where the evaluation method is almost the same as in part two, however, this only deals with the stability. The fourth part introduces the different ways to unbalance the control and gives example of the unbalance control scenario. The final and fifth part gives the example scenarios where the rotor drops on the touchdown bearings. In addition, the fifth part examines what kind of circular orbit responses the rotor performs and what kind of responses are the best for the system.

3.1.1 AMB systems mechanical sizing instructions

The AMB system is strict about the clearances because even a small change between the rotor and magnetic bearing can change the control system from a linear zone to nonlinear. That is why the ISO 14839-4 technical guidelines gives instructions to AMB users and vendors about the magnetic bearings and touchdown bearings design and clearances. (ISO 14839-4, 2012, p. 2-4)

An important part of the designing, is the design specification check list. ISO 14839-4 provides a simple and exact step by step list that will cover all the basic information about the AMB. This check list is seen in appendix III. Using these kinds of tools during the design process will help the customer and vendor to see from one paper the most important facts about the AMB system. (ISO 14839-4, 2012, p. 28)

The clearance and number of magnetic pole-pair (N_p) suggestion about the radial and thrust bearings can be found in the appendices I and II. These provide approximate sizing of the magnetic bearings based on the factor called magnetic force scaling coefficient. This can be calculated from Equation (48),

$$F_0 = \frac{F_{max}}{LB_S^2}, \tag{48}$$

where F_0 is a force scaling coefficient, B_S is a saturated magnetic flux density what is depending on the magnetic material, L is the width of the electromagnet, and F_{max} is a maximum force which can be calculated from the Equation (34). (ISO 14839-4, 2012, p. 24-26)

As mentioned in the chapter 2.1, the proper AMB system includes retainer bearings or touchdown bearings. Instructions for designing a touchdown bearing includes strict clearances and basic layout pictures as shown in appendix IV. According to the ISO standard, the touchdown bearing needs to be designed so that it will protect the system from a limited number of drops, but not for continuous rotation operations, and the designing applications is suggested to follow these bearing mechanisms, (ISO 14839-4, 2012, p. 18)

- Deep groove or duplex pair rolling element bearings for radial support
- Duplex pair rolling element bearings for radial and thrust support
- Solid bushings
- Foil bearings
- The use of different bearing geometry (e.g. cone shaped, tilting pad, pad mounted dry lubricated, etc.)
- A closure-based mechanism for achieving zero clearance
- Hybrids from above

Depending on the rotordynamic modelling methods these different touchdown bearings can be designed to be mounted with an internal damping element or just with a hard mount. More specific information about the touchdown test is covered in chapter 3.1.3. (ISO 14839-4, 2012, p. 18-20)

3.1.2 Vibration analysis and test

ISO 14839-2 determines the vibration test example results and limits. The idea of the vibration test is to make raw lines between different rotating machinery so that machinery with a smaller vibration displacement can be used for longer periods of time than machinery with a larger displacement. Altogether ISO standardization gives four different vibration displacement zones:

- Zone A, contains mostly new machinery with little – or no vibration displacement
- Zone B, machinery which has vibration displacement within this zone is usually considered to be accepted for unrestricted long-term operation.
- Zone C, this machinery is not suitable for continuous long-term operation. But can be used for a short time period at one run.

- Zone D, is machinery that has a large vibration displacement and it can damage itself or can be already damaged

In Table 2, the vibration displacement between each zone is listed. These values are based on the ratio a between minimum value of radial or axial clearance C_{min} and maximum displacement peak D_{max}. (ISO 14839-2, 2004, p. 6-7)

Table 2. Vibration displacement zone limits. (ISO 14839-2, 2004, p. 7)

Zone limit	**Displacement** D_{max}
A/B	< 0,3 C_{min}
B/C	< 0,4 C_{min}
C/D	< 0,5 C_{min}

In order to clarify the different vibration zones in Table 2. Figure 14 can be drawn by using the vibration zone ratios where the difference of the vibration zones are shown by using the rotation speed and displacement. (ISO 14839-2, 2004, p. 7)

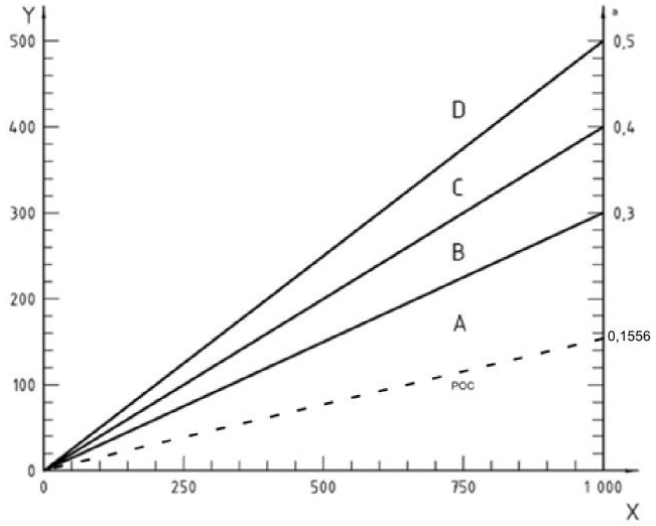

Figure 14. Vibration zones in graph form, where X is minimum or axial clearance C_{min}, Y is maximum peak displacement D_{max} and a is the ratio of $^{D_{max}}/_{C_{min}}$. Also show the illustrative ratio line of PoC AMB system. (ISO 14839-2, 2004, p. 7)

While the measurements are being done, the vibration group of the rotor can been determined by using Equation (49) which is based on Figure 14. (ISO 14839-2, 2004, p. 10)

$$D_{max}/C_{min} < f_c, \tag{49}$$

where D_{max} is determined by using virtual simulation methods or measuring it in the shop test environments. The vibration zone graph, Figure 14, is formed from the ratio of vibration displacement and smallest air gap as a function to the rotating speed. The simulation process itself is simple, but it requires a proper FE-model of the rotor which makes the different vibration characteristics possible. (ISO 14839-2, 2004, p. 10)

3.1.3 Stability margin

An important feature which the ISO 14839-3 provides is a method of evaluating the stability margin in the AMB system. The purpose of this method is to ensure that the system is strong enough to resist changes in the gain and phase margins in the electrical actuators during normal steady-state operation in shop or in field conditions. (ISO 14839-3, 2006, p. 1)

When speaking of the stability margin it usually requires a function called the sensitivity function. The sensitivity function can be described in many different ways but Nyqvist plot and Bode plot forms are probably the most common. However, when evaluating the stability margin with the method that ISO 14839-3, gives the Bode plot is the correct form. The sensitivity function can be determined by two different means. The first way is more analytical, shown in Equation (50), and requires determining the system open loop transfer function $G_0(s)$. This method is based on the inverse value of $1 + G_0(s)$. Ideally $G_0(s)$ should be large then the result of the function is closer to zero and the system has greater stability margin. (ISO 14839-3, 2006, p. 8-11)

$$G_S(s) = \frac{1}{1 + G_0(s)} \tag{50}$$

The second method is based on the experimental measurements that are relatively simple to implement as the AMB system can provide excitations by itself. This feature is used to set an outside excitation, $E(s)$, which is formed as a harmonic or random signal. However,

excitation has to be set in the right place when the signal goes around the system and the response signal V_1 can be measured. The ratio of these two signals, presented by Equation (51), forms the sensitivity function $G_S(s)$. Figure 15 shows the example of the AMB system measurement points, and the closed-loop block diagram system. (ISO 14839-3, 2006, p. 8)

$$G_S(s) = \frac{V_1(s)}{E(s)} \tag{51}$$

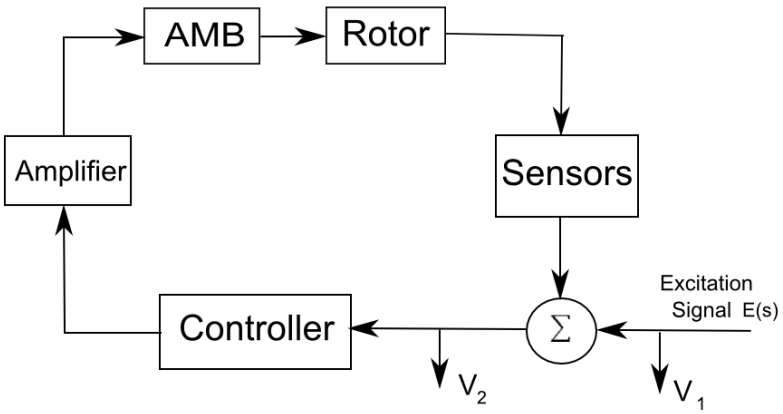

Figure 15. AMB system block diagram with sensitivity function measurement points marked as V_1 and V_2. (ISO 14839-3, 2006, p. 10)

The stability margin can be evaluated with the same basic principles as the vibration analysis. This method is based on the stability zones and the bode plot of the sensitivity function. In Table 3, the different stability zones are sorted by the value of the highest peak in the sensitivity function $G_S(s)$ value. In this table, there are also examples of the type of machinery applications which would be suitable for the stability zone. (ISO 14839-3, 2006, p. 10-11)

Table 3. Stability margin zones with boundaries and description of machinery in each zone. (ISO 14839-3, 2006, p. 11)

Stability zone	**Boundaries [dB]**	**Machinery**
A	$G_S^{max}(s) < 9.5$	New machinery
B	$9.5 \leq G_S^{max}(s) < 12$	Machinery for long-term operation
C	$12 \leq G_S^{max}(s) < 14$	Old machinery with high vibration
D	$14 \leq G_S^{max}(s)$	Already damaged or machine damage expected

The final step of the evaluating method is to form a Bode plot from the sensitivity function when it appears that this specific plot has different instability peaks when compared to the stability zone limits. This method only uses the positive instability peaks from the X–axis. In Figure 16, an example plot is presented of the AMB system with the different stability zones and limits. (ISO 14839-3, 2006, p. 12)

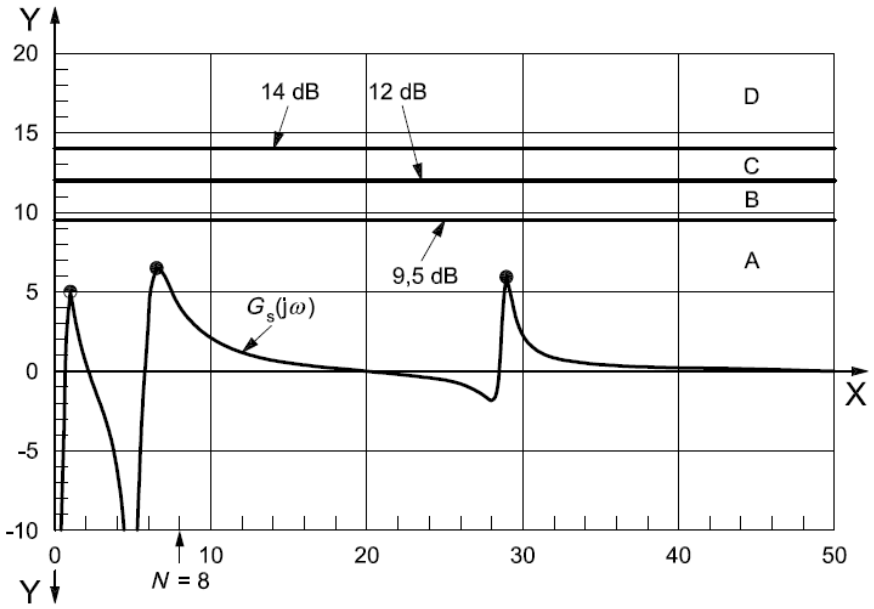

Figure 16. Example of stability margin analysis where Y is sensitivity gain in [dB], X is non-dimensional rotational speed and A, B, C and D is the stability zones (ISO 14839-3, 2006, p. 12)

3.1.4 Unbalance control

The AMB system has unique features, as mentioned earlier on this study, which makes it possible that the balancing quality of the system can usually be lower than those systems with conventional bearing solutions. Typically, this means that a speed-dependent balancing quality judgment is not mandatory. Therefore, the application of quality grades can be too stringent for an AMB system in normal operation, i.e. below bending mode critical speeds. These quality grades are determined in the ISO 1940-1 standard. (ISO 14839-4, 2012, p. 16)

The AMB system should be designed in a way that it can face the situation where the rotating rotor drops into the touchdown bearings. In this situation, low residual unbalance levels helps to minimize touchdown bearing wear and allows faster recovery to the whole system including the magnetic bearings, which might have faced the overload caused by the impact. (ISO 14839-4, 2012, p. 16). These kinds of hazardous situations can be mainly evaded by using a good unbalance control system. This unbalance control system can take advantage of the AMB system feature which adaptively counteracts the rotor vibration response due to unbalance, and which is not possible with conventional ball, air or fluid film bearings. This feature takes effect in three different ways.

- Cancellation or rejection of the synchronous bearing reaction force that allows the rotor to spin around its inertia axis – the limitation is the rotor housing clearances
- Cancellation or rejection of unbalance vibration that compensates for the residual unbalance so that the synchronous rotor vibration is minimized at the transducer locations.
- The system generates more damping force for the exceeding the bending critical speeds

These three effects are the methods for performing the unbalance control. Each method has their own unique characteristics which are listed in Table 4, and it can also be seen that the first control method is the most universal. This method can be used almost in any situation and it has many good features, however, on the other hand this method cannot be applied to the bending resonance speed because the adaptive control methods do not follow the sensitivity function gain peaks. This is the reason why these methods in Table 4 can be used together. Another feature of these methods is that the control system can be tuned to use all

the methods, when facing problems the system can use different methods and then return back to the universal control method. (ISO 14839-4, 2012, p. 35-36)

Table 4. Unbalance control vocabulary and control method properties. (ISO 14839-4, 2012, p. 36)

Unbalance control strategy	**Control system terms used in industry/literature**	**Resulting control system properties**
Cancellation/rejection of synchronous bearing reaction force	- Unbalance compensation - Automatic balancing control - Adaptive vibration control - Adaptive unbalance control - Unbalance force rejection control (UFRC)	- Elimination of synchronous bearing reaction forces - Reduction of housing vibration - Reduction of machine noise emissions - Reduction of power consumption - Avoidance of dynamic power amplifier - Cost reduction - Cannot be applied when passing bending resonance speeds
Cancellation/rejection of unbalance vibration	- Unbalance force counteracting control (UFCC) - Peak gain control	- Damping of unbalance- induced vibrations - May require high bearing force and/or high amplifier power when dealing with near bending resonance speeds - Good for high-precision positioning applications
Damping force generating	- Optimum damping control (ODC)	- Vibration reduction offers fast damping force when passing through bending resonance speeds - May require high bearing force and high amplifier power when dealing with large residual rotor unbalance

As mentioned, the UFRC control method is the most common in the AMB system. Therefore in Figure 17, an example case is presented of the unbalance system control where UFRC topology has been chosen to control and to minimize synchronous bearing force response current, rather than synchronous rotor displacement. Unbalance control analysis can be divided into four different parts a) b) c) and d). A) is the displacement figure which shows the change of the rotors displacement during the unbalance control test. This shows clearly the point, marked as *a* in Figure 17, when the UFRC control is turned on and the rotor's displacement drops from around 25 µm to 15 µm. B) indicates the amount of current used in the function of time which drops radically from 0,38 A to approximately 0,06 A. The change may be considerable with this example, but in general the number of changes in

systems displacement and current depends on the system's specifications and more specifically on the control system and operating speed. However, whatever system is used, it will be improved by using proper unbalance control methods. (ISO 14839-4, 2012, p. 37-38)

The last two parts of the unbalance control analysis, Figure 17, are c) and b). These figures show the Fast Fourier Transform (FFT) diagrams demonstrating the magnetic bearing synchronous current during the unbalance test. When comparing these diagrams, it can be seen that the synchronous current of the system drops almost to zero and the machines noise becomes much lower when activating the UFRC control. The remaining peaks shown in diagrams are formed from measurement and control noise. (ISO 14839-4, 2012, p. 37-38)

Unbalance control needs to be calculated carefully before applying it on a real system because in the worst case scenario where the wrong control type has been chosen it can make the system much worse than without any unbalance controller. However, from Figure 17, it can be seen that with the right controller component choice, from Table 4, the unbalance control makes the system more stable and therefore the system's estimated life time increases. (ISO 14839-4, 2012, p.)

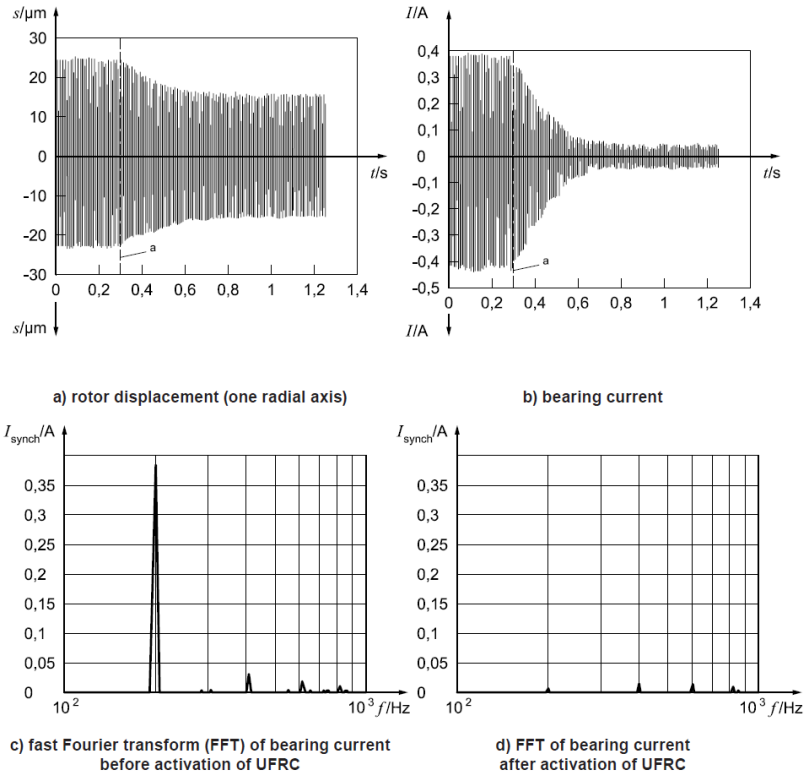

Figure 17. Example system of the UFRC method results, where *f* is frequency, *I* is bearing current, I_{synch} is synchronous bearing current, s is radial rotor displacement in [µm], *t* is time and a is the UFRC control activation point. (ISO 14839-4, 2012, p. 38)

3.1.5 Touchdown test

The touchdown test is always a risk for the AMB system, but with proper testing methods and conditions given by the ISO standard and bearing manufacturers, the touchdown bearings may survive at least three initial touchdown tests in operating conditions given by IEC 60721-4 standard. (ISO 14839-4, 2012, p. 10-20)

When performing the touchdown test, the rotor may exhibit three different types of orbit responses depending on the touchdown bearings designs, the load capacity, and the touchdown bearing damping type. The first one is the pendulum vibration in the clearance space which occurs when the dynamic forces are lower than the static loads. The second is the combined rub and bouncing which occurs when the dynamic forces are higher than the static loads. The final response is the full rub, which is basically backward or forward whirling. When measuring the rotor orbit response the stator and rotor compliance should be taken into account because the orbits of the rotor may be larger than those that are

evaluated from the geometric constants. The different type of rotor orbit responses are found in appendix V. (ISO 14839-4, 2012, p. 18-21)

While the rotor orbit responses are the most important measurement, there are one or two other points which are good to measure during the touchdown test. A vibration analysis and test should be calculated from beginning to end, because the touchdown test itself is a strongly transitional examination. The test should be repeated several times because the confirmation of the system's damping and stiffness factors may be difficult in the workshop test. However, when using simulation methods for these two factors it is good to have them as one output value. (ISO 14839-4, 2012, p. 21)

The touchdown test starts by accelerating the rotor speed to maximum operating speed while the vibration test starts at the same time. After reaching the maximum operating speed, the rotor is dropped from a levitating position to the touchdown bearings. In the shop conditions, it is good to use a method where the rotor is used partially levitated during the coast-down to achieve a reasonable heat exchange between the rotor and the touchdown bearings. In Figure 15, an example touchdown test is shown with a partial levitation method. (ISO 14839-4, 2012, p. 30)

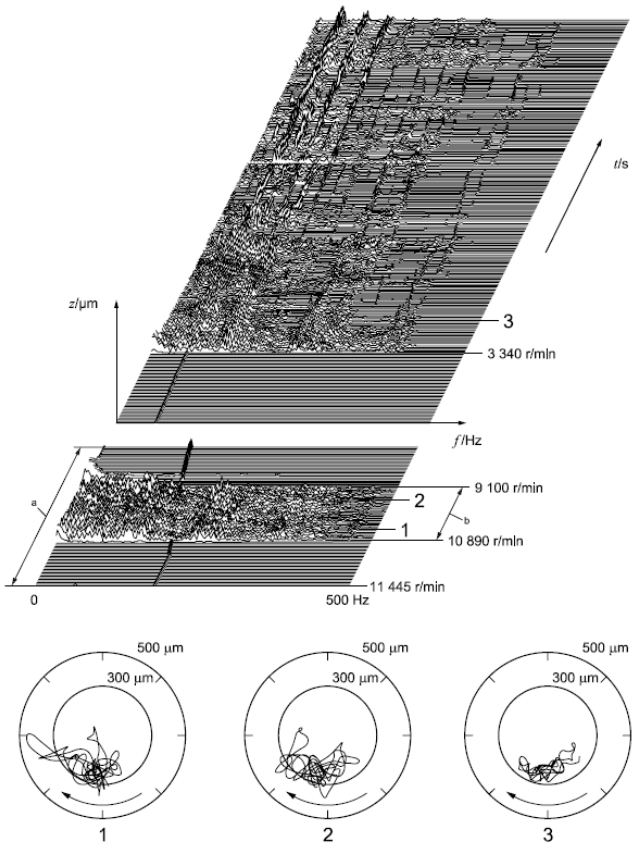

Figure 18. Example of a touchdown test, where a is 90 lines per 24 s., b is 9 s, *f* is frequency, t is time and z is displacement. (ISO 14839-4, 2012, p. 31)

3.2 API 617 standard

The API standardizing organization has released the 617 standard that contains information about axial and centrifugal compressors and expander-compressors for the Petroleum, Chemical, and Gas Industry Services. This standard includes more information about fluid film bearings in fast rotating machinery. However, in the appendix section is more information about application considerations for active magnetic bearings. (API 617, 2002.)

This chapter is divided into two different parts, where the first part introduces the system design, the radial and axial AMB, and the criteria. This section also contains information about the methods used to design touchdown bearing and the requirements of the bearing cartridge.

The second part contains information about the performance tests of the newly commissioned AMB system; firstly, in shop conditions and lastly in operation field

conditions. These tests include; the visual and burn time analysis of the electrical system, the vibration analysis using the machine running test: a comparison of the displacement to the minimum radial clearance, and the touchdown test with two initial drops, and the finishing test with a visual inspection. The last test of the AMB system will take place in the field conditions, this test is quite similar to the machine running test in the shop conditions, but there are some more factors that can affect the maximum allowance of displacement.

3.2.1 System designing

The API 617 standard insists that the AMB system, and even the touchdown bearings, have to be designed and constructed in a way that their service life will be a minimum of 20 years with interruptions, and 5 years of constant operating time without any interruptions. A typical system contains the following parts

- Bearing and sensor rotor lamination stacks (two per rotor)
- Radial magnetic bearing stator assemblies (two per system)
- Axial magnetic bearing assemblies (two per system)
- Radial and axial position sensors and any associated electronics.
- Touchdown bearings for radial and axial loads, including the damping mechanism.
- Speed probes (two per each set)
- Control system cabinet (normally one per system)
- Proper product data management

As all the components have to be suitable for operation both in shop tunings and field conditions it requires that all the sensors have to be suitable for brief exposure to hydrocarbon liquids. In addition, the electrical heat insulation of the stator windings have to be class H (180 ^{O}C) and the overall system assembly heat insulation has to be class F (155 ^{O}C) to prevent unnecessary electrical or magnetic damage. Keeping an eye on the system maintenance requires that all leads have to be identified with durable markings from both the stator and the connector end, as this will make the maintenance easier, faster and safer for both user and the system. (API 617, 2002, p. 4- 41)

The mechanical part of the system and load capacity of the radial and axial magnetic bearings need to be designed in a way that prevents contact between any part of the stator and the

rotor parts anywhere in the speed the range. While the unit must be capable of running continuously from zero to trip speed with steady aerodynamic slide loads at each impeller equivalent to 4 % of the total torque of the system in any part of the speed range. The electrical part of the radial magnetic bearing requires a minimum of two different sensors, two removable and replaceable temperature sensors, and two radial position sensors. Temperature sensors have to be installed in each upper part of the radial bearing where one is protection against excess temperature and the other is a backup sensor; the radial position sensors have to be installed as close to the radial bearing as possible. (API 617, 2002, p. 4-41)

The load capacity of the axial magnetic bearing needs to be designed so that the rotor does not touch the stator or the touchdown bearings at any operation speed or in any operation conditions. In case the system contains an automatic thrust equalizing control system then the magnetic bearing needs to be at least twice the largest residual thrust expected using the automatic thrust equalizing system. An axial bearing uses the same amount and same sensor principles as the radial bearing mentioned above. (API 617, 2002, p. 4- 41-42)

The AMB system needs to have two touchdown bearings located in each end of the rotor where the touchdown bearing cartridge is easy to install. The cartridge usually contains cageless ball bearings, which are ceramic balls with steel races. However, in different applications the bearings can be of different materials or a completely different type. In addition the cartridge contains the damping mechanism, if required, to prevent destructive whirl during the touchdown. (API 617, 2002, p. 4-42)

Overall, the touchdown bearing system needs to survive at least two touchdown tests from the maximum operation speed to zero speed with the normal aerodynamic braking and nominal process induced thrust load, which should be lower than 75 % of the thrust bearings load capacity, or else they need to survive at least ten momentary contacts caused by temporary disturbances in the system. This contact weakens the electromagnets capacity where the magnitude of the overload exceeds the magnetic bearing force by 25 % during 0.5 sec. (API 617, 2002, p. 4-42)

3.2.2 AMB system's performance test in shop and field conditions

The API standard gives instructions as to what the vendor needs to do before delivering the AMB system to the customer. There are a series of tests conducted on the mechanical and electrical systems which need to be performed in shop conditions. (API 617, 2002, p. 4-43)

Electrical components need to have a 24-hour long burn-in prior - this means that all components are subjected to high-temperature treatment to make sure that there are no faults in manufacturing process. Moreover, the control system has to be tested completely with computers and by test runs in shop conditions before delivery. (API 617, 2002, p. 4-43)

The rotor assembly in the AMB system needs to pass the mechanical maximum operation speed running test in shop conditions. The API standard indicates that the maximum deformation displacement of the rotor from the center of the touchdown bearing to any given levitation axis is 0.3 times the minimum radial clearance between the rotor and touchdown bearing. The total displacement is the sum of the different components, for example, the shaft vibration peaks, the casing distortion, and the aerodynamic loading, etc. These components can be measured with a simulation verification process or in practical measurements during the test. If the manufacturer of the system has given different values for the maximum displacement they must be smaller than 0.3 times the minimum radial clearance. (API 617, 2002, p. 4-43)

The final test in the shop conditions is the touchdown test where the goal is to monitor whether the touchdown bearings are acceptable for long term operating purposes. Touchdown tests have to be performed with different touchdown bearings than the real machines, because this test damages the bearings every time and shortens the expected lifetime. The touchdown test begins with an acceleration of the rotor to the same operation speed required from the AMB system by the application. After this the rotor is dropped for a 3 second period, then re-levitated again. After that the system will be stopped and the clearances have to be checked with electronics. If the clearances are still in the tolerance range the machine is accelerated again and rotor will be dropped, however this second drop is 1 second long. (API 617, 2002, p. 4-43)

After the second touchdown test the AMB system needs to be disassembled and inspected. The touchdown test is successful and the system approved if after the shop test there is no sign of damage in the magnetic bearing assemblies. However, the touchdown bearing assemblies need to be changed when assembling the system again because the landing surfaces and touchdown bearing assemblies are not the main evaluation component in the AMB system. (API 617, 2002, p. 4- 43-44)

The API 617 standard states that newly commissioned AMB systems have to be inspected and tested once, and also in the system's proposed operating field conditions. This test is very similar to the mechanical running test performed in the shop conditions, but in the field the maximum allowable of rotor movement is 0.4 times the minimum radial clearance, instead of the 0.3 required in the shop condition test. The reason to for this larger allowance limit is that in the field operating conditions the power levels are typically higher than in the shop conditions, and fewer variables are controlled. That is why it is better to permit little more allowance in the field than in low power shop tests. (API 617, 2002, p. 4-42)

3.3 Discussion regarding the API and ISO standard

From these two major AMB system standard sets, ISO 14839 and API 617, the ISO standard provides a better overview off the whole machinery; especially after the ISO organization released the new ISO 14839-4 technical guidelines section. However, the API 617 standard provides quite a good overview for the AMB system but specific information about the mechanical system with figures and tables is omitted.

There are many similarities between the two standards; the first, being the maximum vibration tolerance level. The ISO standard uses the vibration zone method where the maximum amount of peak displacement for machinery suitable for long term operations is 0.4 times the minimum radial clearance. Moreover, if this value is compared to the displacement limit given by API in the field conditions it is exactly the same 0.4 times minimum radial clearance. Therefore the vibration test can be performed using the method given by The ISO standard in Chapter 3.1.2.

Touchdown bearings are an important part of both standards but in the ISO 14839-4 standard provides good clearance tables and figures, see appendix IV, which explains the problem

better than API 617 method which explains everything in plain text. However, the method as to how the touchdown test should be performed is quite different in these two standard organizations. The ISO standard method is more analytical and can be performed by using both simulation methods and shop test methods while the API can be performed with real machines and requires a full visual inspection after the test. Both methods work but in most scenarios the ISO method is more universal and can be applied in prototypes better than the API method.

The ISO 14839-3 describes a good method for evaluating the stability margin which should be done for every AMB system to make sure that the system has a reasonable stability margin. The API standard does not have a direct analysis for the AMB systems but the API 617 standard has a method called level I stability which can be modified to be suitable for AMB machinery. (API 617, 2002, p. 1-19) Nevertheless, the method given by the ISO standard is simpler way to evaluate the stability margin than methods given by API.

Overall, the ISO standard provides better simulation possibilities and more specific information for analysis, therefore, in the subsequent chapters the methods used are taken from the ISO 14839 standard. As mentioned, API provides a good overview of the AMB systems, but specific and detailed information is omitted and that is the reason why it has remained only at the informative level of this study.

4 VERIFICATION OF THE AMB SYSTEM UNDER DESIGN

This chapter contains the practical part of the study and this chapter is divided into three different parts. The first part introduces the AMB system and shows the basic layout of the whole AMB system and then provides a simplified model, which is used to make the verification simulations. The second part deals with the product data management using the methods given by the ISO 14839-4 standard, and this provides the design specification table. In addition, this part introduces all the information concerning the simulation process requirements. The other important subject of this chapter is the simulation and system verifying process. In section 4.2, the results of the system simulation are shown by using different diagrams and standardized methods from chapter 3.

4.1 Introducing the system

PoC or Proof of Concept is a project created by HS-EDEN. This AMB system is still in a concept level. From Figure 19, the basic cut assembly figure can be seen, which includes all the components that have been introduced in the previous chapters.

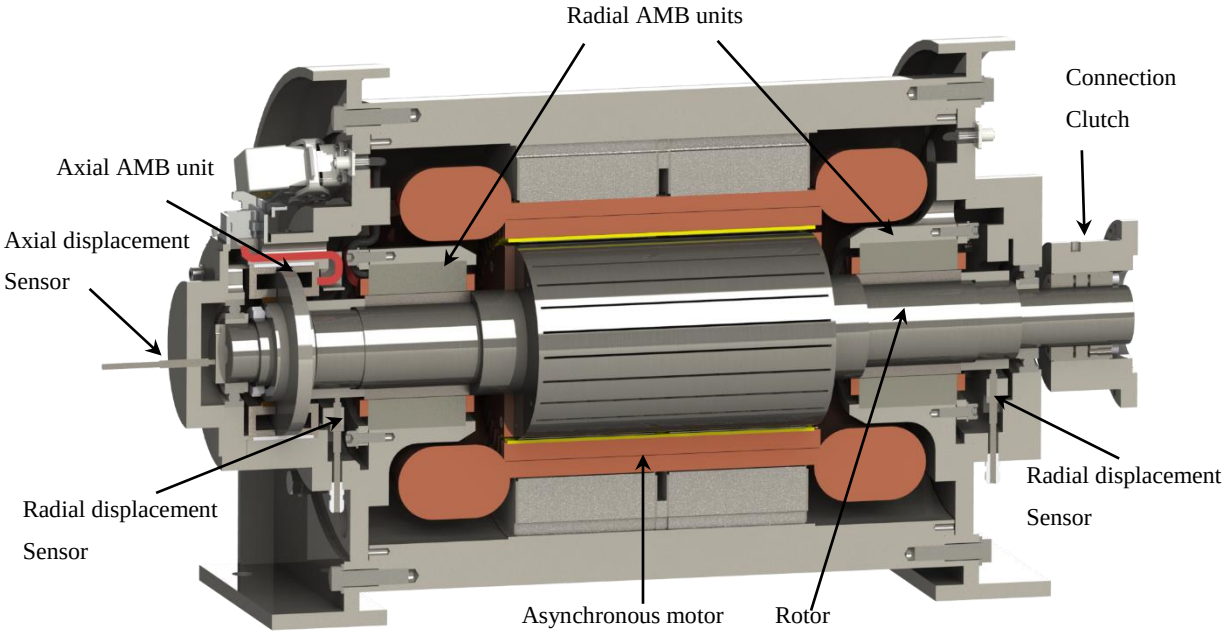

Figure 19. Layout figure from the PoC naming all the main AMB components.

The whole system is complex and has many detailed points, but for the simulation process system these are simplified to the rotor, the radial AMB sockets, the axial AMB rigid disk and the connection clutch. These parts can be modeled in a RoBeDyn program to have simplified system that is easier to study than the whole complex system, Figure 20. The schematic of the studied rotor can be seen in Figure 21, where the location of AMBs, retainer bearings, and the main measurements of the rotor are shown.

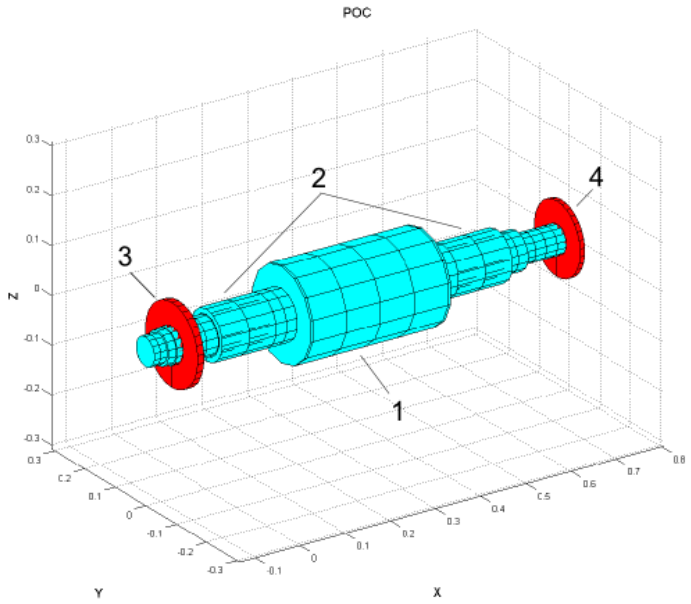

Figure 20. Simplified 3D rotor model from RoBeDyn. Where 1 is the rotor, 2 shows the radial AMB places, 3 is the axial AMB and finally 4 is the connection gear.

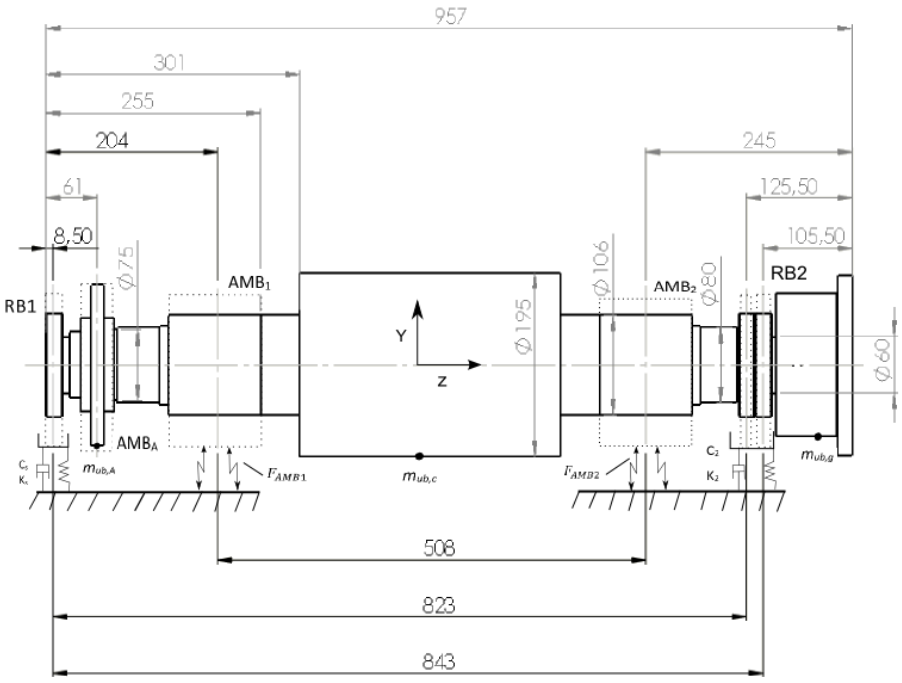

Figure 21. Schematic figure of the simplified system, where RB1 and RB2 are Retainer Bearings, C_s is damping of the support element, K_s is the stiffness of support element. Radial AMB 1 force is F_{AMB1} and radial AMB 2 force is F_{AMB2}. Location of the unbalance masses is marked as $m_{ub,A}$, $m_{ub,c}$, and $m_{ub.g.}$

The greatest differences in the rotor between the whole system, Figure 19, and the simplified model, Figure 20, are the connection clutch and axial AMB rigid disk. Both parts are modeled in a simplified model with simple masses and disks. These disks have the same polar inertia properties as the actual parts. This method reduces the chance of calculation error because the joint elements could have a different displacement in a simulation than in a real system.

The simplified model is verified by using the SolidWorks frequency simulation and then the results are compared to the simulation free-free mode diagram, Table 5. These modal frequencies are in a 10 % margin of each other, and it can be said that the models are the same. (Heikkinen, 2014).

Table 5. Modal frequency difference comparison of RoBeDyn and SolidWorks

Mode	RoBeDyn [Hz]	SolidWorks [Hz]	Difference [%]
1	555.1 Hz	534.95 Hz	3.76 %
2	555.4 Hz	535.49 Hz	3.72 %
3	1106 Hz	1081.5 Hz	2.26 %
4	1107 Hz	1082.3 Hz	2.28 %
5	1625 Hz	1679.6 Hz	3.36 %
6	1626 Hz	1682.1 Hz	3.44 %
7	2928 Hz	2853 Hz	2.62 %
8	2928 Hz	2920 Hz	2.74 %

From Table 5, it can be seen that the modal frequencies are close to each other. The main reason for differences to occur is that RoBeDyn uses beam elements to calculate the rotor-dynamic systems and SolidWorks uses 3D solid elements. However, the model parameters can be adjusted, but the effect is small and the frequencies are within a 10 % margin, consequently it is better to use the RoBeDyn model in further simulation process. In Figure 22 is shown the mode shapes from RoBeDyn, where can be seen how the different mode shapes goes along the rotor.

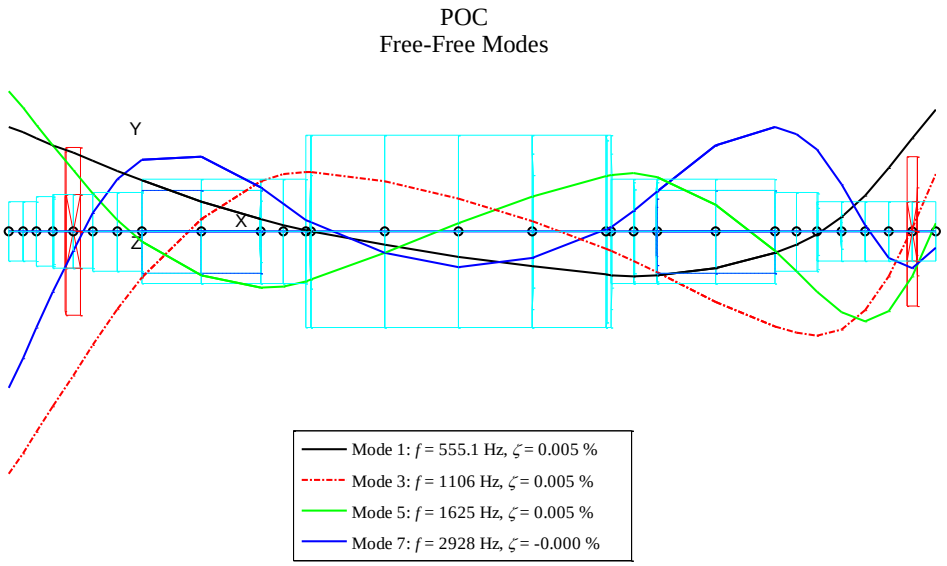

Figure 22. Modal frequency diagram from the RoBeDyn program.

4.2 The standardized design specifications list and material specifications

Design specifications have been collected into one place from different instances of research. Table 6 shows the material properties of the rotor, which are important with this study, and it can be seen form Table 6 that the rotor is built from two different alloys. The S355JO alloy owns good magnetic properties and is designed to be part of the bearing assemblies. However, the alloy has better strength properties so it is used in the main rotor and in the connection gear part.

Table 6. Properties of the system's material.

	Property	Value
	Rotor and connection gear	
1	Young's modulus, *E*	200 GPa
2	Density, ρ	7850 $^{kg}/_{m^3}$
3	Poisson's Ratio, ν	0.3
4	Rotor mass, *m*	92.5 kg
5	Connection clutch mass, *m*	9.26 kg
	Radial AMB sockets and axial AMB disk, S355JO	
6	Young's modulus, *E*	210 GPa
7	Density, ρ	7800 $^{kg}/_{m^3}$
8	Poisson's Ratio, ν	0.28
9	Radial AMB socket mass, *m*	1.87 kg
10	Axial AMB disk mass, *m*	2.83 kg

In chapter 3.1.1, the AMB systems mechanical sizing instructions were referred to in the standardized design specifications list. Table 7 presents this list completed with all the known information about the prototype system. Most of this information is crucial for the simulation and the model verifications, but there are also parts that are useful for the dealers and customers. From Table 7, is can also be seen that the machines environment properties cannot be completed because the prototype has not been fully manufactured. Furthermore, another large area that contains unknown information is the Load Definitions section. There are also smaller parts of whole table that cannot be completed yet.

In future, when it is possible to updated and fully complete this table, it will become a useful tool for further model verification. It will also mean that the important specifications are kept in one place, for better and easier access.

Table 7. Standardized design specification checklist for HS-EDEN PoC prototype AMB system. (ISO 14839-4, 2012, p. 28)

	Machine	
1	Type	AMB system
2	Customer	-
3	End user	-
4	New design/retrofit	New design
	General characteristics	
5	Operating speed range	4000 – 15200 r/min
6	Nominal speed	15200 r/min
7	TRIP speed	18000 r/min
8	Orientation (Horizontal/vertical/any)	Horizontal
9	Power at nominal speed	500 kW
10	Rotor weight	106.46 kg
11	Rotor length	950 mm
12	Balance quality	2,5 G
13	Nature of process fluid	-
	Machine environment	
14	Internal medium (air/vac/fluid)	Temp.: - ^{O}C, Pressure: - kPa
	Other info (composition/corrosion/humidity/etc.)	-
	Available cooling medium (water/air/other/none)	-
15	External medium (air/vac/other/none)	Temp.: - ^{O}C, Pressure: - kPa
	Other info (composition/corrosion/humidity/etc.)	-
	Available cooling medium (water/air/other/none)	-
16	Electronic cabinet environment	Temp.: - ^{O}C, Pressure: - kPa
	Distance to machine	- m
	Back-up batteries	-
	Back up time	- min
	Load Definition	
17	Assembly drawing	POC S107969
18	Static process load (radial)	N Axial location: - mm
19	Static process load (thrust)	N Axial location: - mm
20	Dynamic process load (radial)	N Axial location: - mm
	Frequency	- Hz
21	Dynamic process load (thrust)	N Axial location: - mm
	Frequency	- Hz
22	Additional dynamic load margin (radial)	N
23	Additional dynamic load margin (thrust)	N
	Touchdown bearing	
24	Supplied by (vendor/customer)	-
25	Type (ball bearings/other)	Ball bearings
26	Mounting (resilient/hard)	Hard
	Speed sensor	
27	Supplied by (vendor/customer	-
28	Type (Hall effect/optical/other)	Hall effect

4.3 Simulation

As mentioned previously, this part includes the systems simulation results which have been obtained using the instructions given in the ISO standard. This section can be divided into three different areas. The first area is the vibration and unbalance response analysis and these two sections are dealt together instead separately, because the RoBeDyn models give an unbalance measurement in form where the vibration analysis can be done directly. The unbalance response itself is limited to the analysis of the control system.

The second part deals with the stability margin. The Matlab functions and RoBeDyn models are used in this simulation to perform the transfer function which can be plotted.

The final part of this simulation chapter deals with the touchdown bearings, where a modified RoBeDyn program is used to verify the characteristics of the touchdown bearings. The simulation itself is made by using the information introduced in chapter 3.1.5 and the orbit response research is done by comparing the results of simulation to the different orbit responses introduced in appendix V.

4.3.1 Vibration and unbalance response analysis

Vibration analysis model uses a closed loop UFRC unbalance control system, the properties of which can be seen in Table 4. The MIMO LQG control system and the full theories behind the AMB system model where the RoBeDyn model is based can be found in Introduction to Dynamics of Rotor-bearing System (Chen, 2005). In Table 8, is the controllable variables of the control system are introduced and also the variables that were used to simulate the whole system

Table 8. Controller specifications.

Property	Value
Bandwidth, w_n	25 Hz
Damping value, ψ	0.222
Bearing current stiffness, K_i	219.6 $^{N}/_{A}$
Bearing position stiffness, K_s	$2.57 \cdot 10^{6}$ $^{N}/_{m}$
Speed range, $\Delta\boldsymbol{\omega}$	0… 18000 rpm

The unbalance masses of the rotor were evaluated using the SolidWorks simulation. Figure 21 shows three different locations of the unbalance masses. The first unbalance mass is in the axial AMB disk, $m_{ub,A}$, which is assumed to be 1.07 g·mm@180^o. The second unbalance mass is in the center of the rotor, $m_{ub,c}$, which is assumed to be 4.56 g·mm@180^o. The final unbalance mass is located in the connection gear, $m_{ub,g}$, and this mass is 2.78 g·mm@180^0.

A vibration analysis is performed together with the unbalance response. It can be determined using the RoBeDyn as to which the best controller in different applications and a comparison is done with different of vibrations during the operation. Figure 23 presents the best result of the vibration analysis.

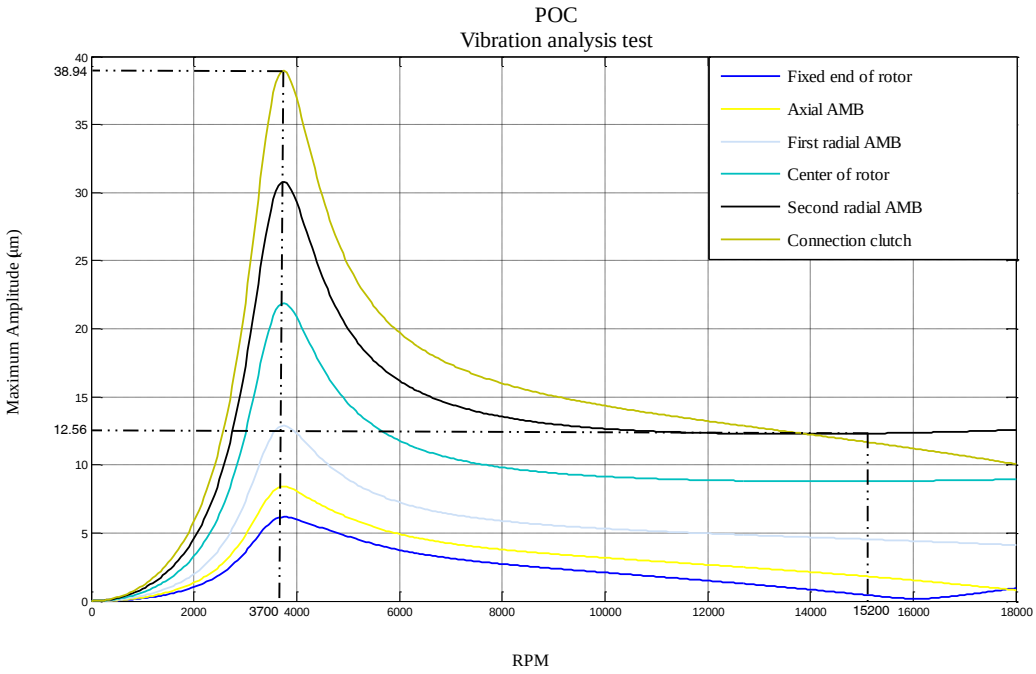

Figure 23. Vibration analysis of PoC from RoBeDyn. Where is shown the highest and lowest displacement peak. There can be seen also, that the rotor deformed shape is conical.

The smallest gap in the PoC system is located in the touchdown bearings and it is 0.25 mm. The highest peak of displacement from the RoBeDyn simulation is 38.94 µm and it is located in the connection gear end of the rotor. Therefore, Equation (49) is used to determine the ratio of the highest peak of displacement and the smallest gap 0.1557. This ratio is considerably below the A zone limit of 0.3 when the systems achieves a vibration zone grade of A, according the ISO 14839-4 standard.

From Figure 23, it can be seen that the displacement peak is located around the 3,700 rpm zone and that the rotor displacement is constantly dropping. When the rotating speed reaches the maximum operation speed of 15,200 rpm the displacement has dropped to its minimal values and even when reaching the maximum trip speed of 18,000 rpm displacement values are in the acceptable zone and seem to rise towards the next displacement peak.

4.3.2 Stability margin analysis

The stability margin requires analysis that needs the whole system to be working together, exactly right. However, the main power is on the controller and its design. This analysis uses the same controller and specifications that are introduced in Table 8 in chapter 4.3.2 ‘’Vibration and unbalance response analysis’’. This analysis is performed with two different controllers and three different cases where the differences between each controller are the number and place of the error measurement points. With this information prober Bode plots can be formed with reasonable accuracy.

Transfer function of the system can be determined by using the state space representation, where the general matrix from is given in Equations (38) and (39). This state space representation is derived from the differential equations that represents the system dynamics. Another way to find the system transfer function was introduced in chapter 3.1.3, where the excitation signal is measured from two different points. In this study the transfer function is measured from the system model from RoBeDyn using the measurement information given by ISO 14839-3 standard. Now continuous-time transfer function $G_0(s)$ can be determined from RoBeDyn as: (Yoon, et. al., 2013. p. 167-170)

$$G_0(s) = \frac{39{,}68s^2 + 2.488 \cdot 10^4 s + 1.025 \cdot 10^5}{0.0001s^2 + s + 0.1} \tag{52}$$

Using the information from Equation (50) system sensitivity function is following:

$$G_s(s) = \frac{0.0001s^2 + s + 0.1}{39{,}68s^2 + 2.488 \cdot 10^4 s + 1.025 \cdot 10^5} \tag{53}$$

This sensitivity function is studied using the standardized methods from ISO 14839-3 standard, which are the base of the RoBeDyn control model. This model uses the theories from MIMO-controller design and PID-controller design. For more specific information about the theories behind the RoBeDyn system control model can be found from Yoon's paper. (ISO 14839-3, 2006) (Yoon, et. al., 2013. p. 167-178)

The first controller and the first case are the SISO based PD-controller where the proportional gain *kp* and the derivative gain k_d, are:

$$k_p = \frac{m \cdot {w_n}^2 + K_s}{K_i} \tag{54}$$

$$k_d = \frac{2 \cdot m \cdot w_n}{K_i \cdot \psi}, \tag{55}$$

where the variables can be seen from Table 8. AMB system which are under PID-controller behaves similar to the system which are under PD-controller. Therefore, it is not uncommon that AMB system have separately tuned PD-controller which is used to achieve the desired stability and transient characteristics. Integral term is added in the control system later to improve the steady-state response. This is the reason why in this study is used the PD-controller instead of PID-controller. (Yoon, et. al., p. 159-160). The response diagram of the PD controller sensitive function is shown in Figure 24. It can be seen that the highest peak in the stability function bode plot is 5.6 dB high which is considerably lower than in the MIMO controllers.

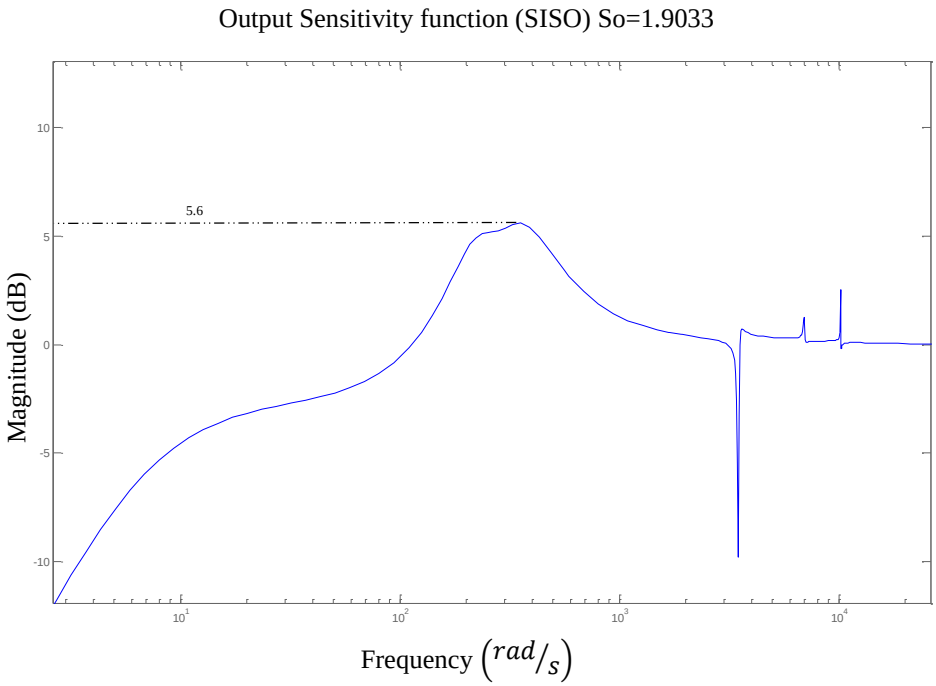

Figure 24. SISO controller stability analysis Bode diagram.

The second controller type is the MIMO-controller which is based on the LQG controller theory. With this controller system, the highest peak in the stability function is 9.48 dB and as it can be seen in Figure 25, it can be located at the same place as in the first case. The MIMO Input-Output (I/O) Bode diagram has two curves. The first curve is the input curve that forms the highest peak. The second curve is the corresponding error curve to the first, but the main difference is that the control system uses this input curve to change the behavior of the system.

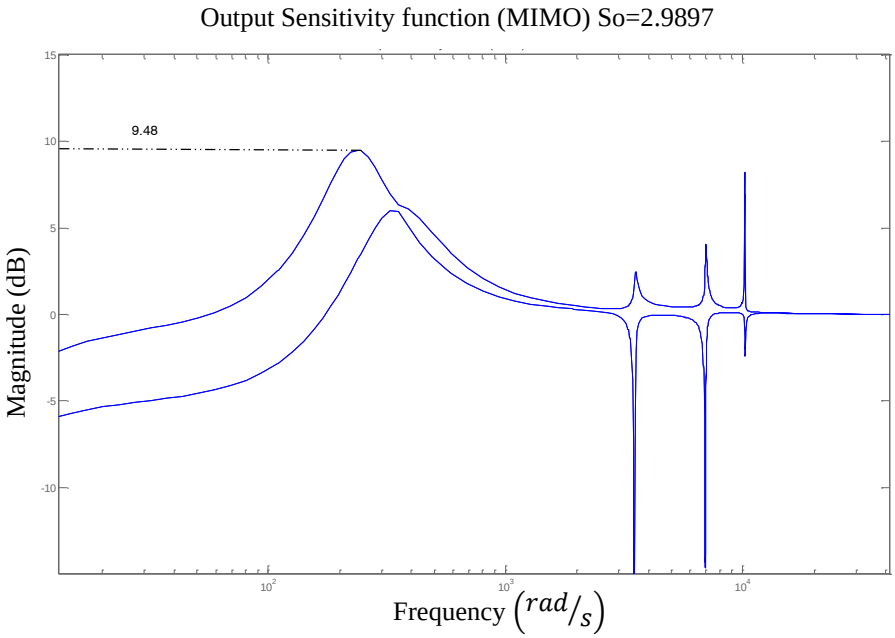

Figure 25. MIMO controller stability analysis Bode diagram.

The controller type is also an MIMO controller, Figure 25, but the main difference to the controller shown in Figure 25 is that at high speed I/O signal has been added. From Figure 26, it can be seen that the displacement peak is located again in the same place and the stabilization peaks are quite low. Even if this controller has more I/O signals the highest stability function displacement peak is only 9.48 dB.

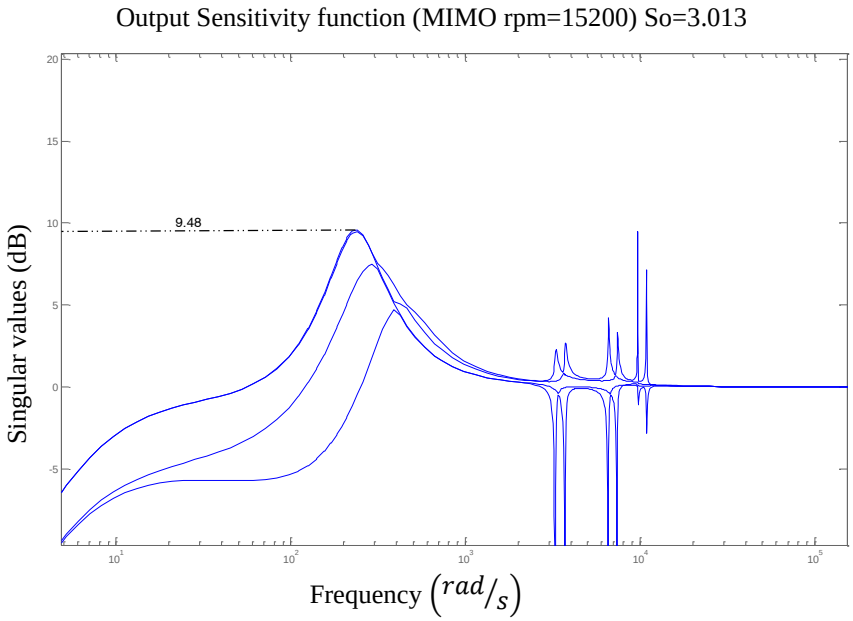

Figure 26. MIMO control with integrated high speed control signal.

From Figures 24 to 26, it can be seen that the highest stability peak with every controller type is 9.48 dB. When analyzing this with the methods given in chapter 3.1.2 ‘’Stability margin’’ it can be said that when stability peaks are lower than 9.50 dB the system receives the stability zone grade A according the ISO 14839-3 standard.

4.3.3 Touchdown test

The final analyze is the touchdown test. Here the rotor is accelerated to 15,000 rpm and then dropped down to the touchdown bearings. The air gap in this system is 250 µm between the rotor and touchdown bearing. This system uses two different touchdown bearings. At the free end of the rotor are 6014 ceramic, deep groove, high precision ball bearing marked with RB1 in the simulation models, and in the fixed end of the rotor there are two 5S-7914UC ceramic, deep groove ball bearings. Marked with RB2 in simulation models (Heikkinen, 2014)

Most of the bearing properties can be found from the NTNs and SKFs catalogues but the manufacturer cannot give the information about the bearing damping coefficient or the different conformity ratios. The reason for this is highly increasing number of attempts to copy the real bearing and piracy in the bearing business. However, these parameters can be evaluated to be closed as possible by using the ISO 16281 standard (Jauhiainen, 2014). All the bearing properties are needed in the Matlab simulation, of these two the bearings safety bearings are presented in Table 9.

Table 9. Touchdown bearing properties. (NTN, 2010, p. 98) (SKF Group, 2014)

Property	6014 (RB1)	5S-7914UC (RB2)
Outer diameter, *D*	70 mm	70 mm
Bore diameter, d_1	110 mm	110 mm
Pitch diameter, d_m	90 mm	85 mm
Width, *B*	20 mm	16 mm
Ball diameter, *D*	12 mm	11.7 mm
Number of balls, *z*	11 pcs.	11 pcs.
Static Load rating, *C0*	$31 \cdot 10^3$N	$20.9 \cdot 10^3$ N
Damping coefficient, c_b	0.30 Ns/mm	0.27 Ns/mm
Internal clearance, C_d	$15 \cdot 10^{-3}$mm	$9 \cdot 10^{-3}$ mm
Conformity ratio in	0.52	0.52
Conformity ratio out	0.52	0.52

The safety bearing system requires a proper support system. This system has different properties that are verified with the SolidWorks 2013 simulation program and calculated with basic DOF vibration equations. In Table 10, the support system properties used are assembled for the touchdown simulation. The first evaluated parameter is the system's stiffness, which requires the maximum displacement value from SolidWorks. With this displacement value the stiffness can be calculated from $K = F/\delta$, where F is known force and δ is the maximum displacement.

The following important part is the efficient mass of the support system which can be solved by comparing the first natural frequency between the SolidWorks 2013 simulation and differential calculation methods. The first natural frequency can be solved from $f = \sqrt{k/m}$, where k is the stiffness of the support system and m is the mass.

Friction between the rotor and bearing inner-ring can only be estimated at this point in the project. In the simulation models the table values for the static friction factor and kinetic friction factor have been used that are estimated to be the lowest in the table values. Accurate values of these factors can be measured after the system is constructed.

The last parameter is the damping factor. This can be evaluated using the definition of the critical damping $C_{cr} = 2\sqrt{k \cdot m}$. Using an estimated damping ratio, $\zeta = {C_{bb}}/{C_{cr}}$, where is know that damping ratio 2 to 5 % is for slightly damped system, 10 to 15 % is moderate damped system and 15 to 20 % is highly damped system.

Table 10. Safety bearing support system parameters.

Property	RB1 Unit	RB2 Unit
Mass factor, m_{eff}	0.772 (6.61 kg)	0.448 (10.16 kg)
Stiffness, *K*	$6.7 \cdot 10^7$ ${N}/{m}$	$3.7 \cdot 10^7$ ${N}/{m}$
Damping, *C*	8417.79 ${Ns}/{m}$	7755.46 ${Ns}/{m}$
Damping ratio, ζ	20 %	20 %
Exponent of the force-deflection relationship, *e*	1.1	1.1
Static friction factor, μ_s	0.11	
Kinetic friction factor, μ_k	0.05	

Backup bearing calculation model is modified version from the original RoBeDyn Matlab calculation script. Unlike the model used in the vibration analysis, this model does not include the unbalance forces. The theories behind the backup bearing calculation model can be found from Halminen's Dropdown event simulation model study. (Halminen, et. al. 2015)

Figure 27 shows the touchdown test y-axis displacement plot. From this plot can be seen that the highest displacement changes are around 0.025 s to 0.1 s. In this time zone the rotor drops from a levitating position and make the first bounces.

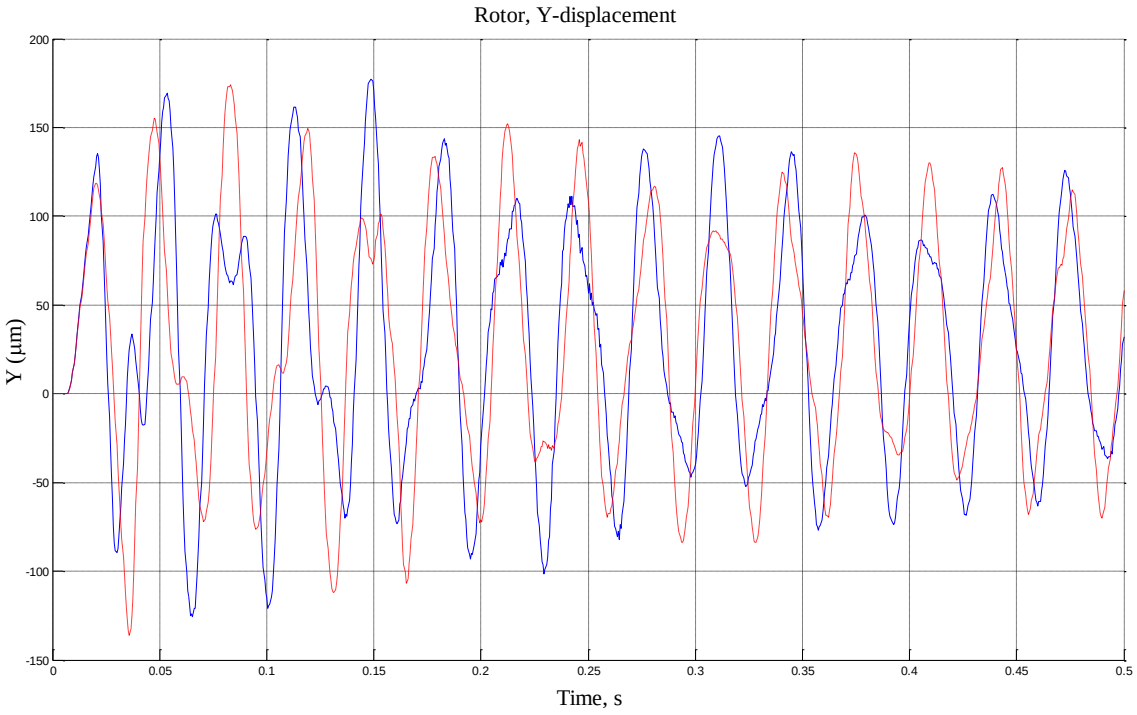

Figure 27. Rotor *y*-axis displacement diagram in the touchdown test. The dashed line is RB1 and continuous line is RB2.

Figure 28 shows the actual rotor orbit response. From this figure it can be seen that the first bounce is the highest and after that the displacement which is shown in Figure 26 is just the spinning movement in the bottom of the touchdown bearing. Overall, the highest displacement bounce is around 120 µm which is little less than half of the air gap between the rotor and stator. However, the model does not have the unbalance forces included which means that in reality the responses will be higher. Figure 28 shows the same rotor responses as in Figure 29, but shows one touchdown bearing at a time.

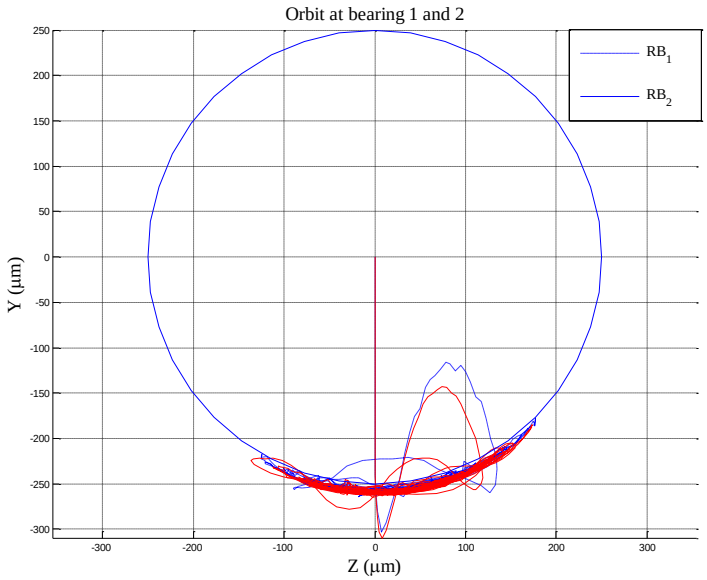

Figure 28. Rotor orbit response of touchdown simulation test. The dashed line is the RB1 bearing and the continuous line is the RB2 bearing.

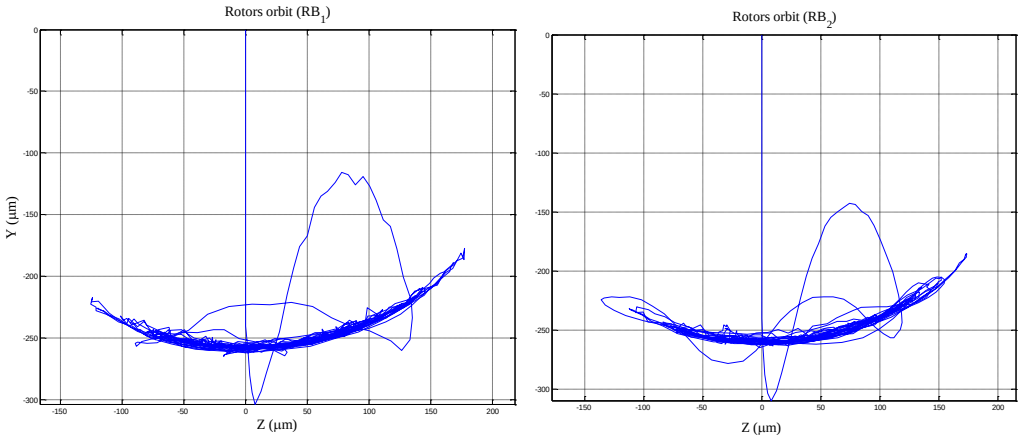

Figure 29. Single touchdown bearing orbit responses. The left side is the RB1 and the right side is the RB2 bearing.

When comparing the results from figure 28 with the ideal rotor orbit response diagram, Figure 30, from ISO 14839-4 standard, it can be said that the results of the simulated touchdown test are acceptable according the ISO 14839-4 standard.

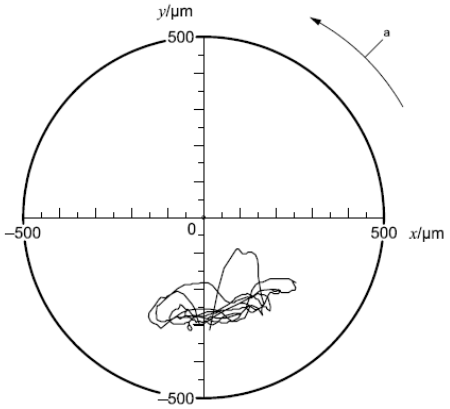

Key
x, y displacement
[a] Rotational direction.
NOTE Measurement duration is 0,2 s.

Figure 30. Standardized orbit response of the rotor touchdown test. (ISO 14839-4, 2012, p. 19)

5 RESULTS

This chapter contains the final conclusions of the studied results from chapter 4. This chapter can be divided into two separate parts, the first part reporting what the main results are and whether they answer the main goal of this study. The second part is more abstract because it deals with the side results which have come from studying process and the listing of them.

5.1 Key results

The main goal of this study was to provide the information about the standardized AMB system verification methods and put them into the practical use. The theory of the standardized methods has been provided in chapter 3, where the verification methods are the following;

- Clearance and geometrical inspection
- Vibration analysis
- Stability margin analysis
- Unbalance control
- Touchdown test

Using these verifying methods the HS-EDEN PoC concept of the AMB system can be verified, and this was one of the main issue of this study. During the verification process the AMB system was compared to the standardized system preferences. After all the processing, the system passed all the verifications at the concept level and it can now be said that the concept level system is approved according the ISO 14839 standard.

5.1.1 New information produced

To complete the verification process system, it needed to be modeled in RoBeDyn. Therefore, these RoBeDyn simulation models are universal for this system and available to every Matlab user in the HS-EDEN project. In future, these models will help designers to model the system faster so that their concentration can be focused on the different goals others than the modeling or verification processes.

The important information about this specific system are the results of the different verification methods, starting with the vibration analysis, where the highest peak of the rotor displacement is 38.94 μm. The second important part is the behavior of the system during the touchdown test, which provided a considerable amount of new information regarding the PoC system. Lastly, the stability analysis gave information about the controller designs and confirmed that in theoretical situations the controller works well.

5.2 Side results

This study has already fulfilled the requirements as regards the main goal and providing new information. However, one or two smaller points have arisen which could be called side results.

One noticeable piece of information was that API 617 and ISO 14839 standards give very similar guidelines to the verifying process of the AMB system. However, as in chapter 3.3 ‘‘Discussion between API and ISO standard’’ it can be seen that the ISO standard gives more detailed information about the AMB systems than API.

During the verification process there were noticeable points in the parameter defining, especially in the touchdown bearing system, where it was necessary to find the damping ratios and race comfort ratios. These parameters were difficult to obtain even from the bearing manufacturer, however, these parameters can be measured and a result obtained that is as close as possible to the real values.

6 DISCUSSION

This chapter is divided into four different parts, where the main goal of this chapter is to discuss the reliability of the study. The first part discusses the objectivity of the study, and the second part deals with the reliability and possible errors; which are the most important facts from the initial values of the study. In the third part of this chapter, is the values and possible applications are introduced that have produced new information. Finally, the fourth part gives suggestions as to future research areas and suggestions for future AMB verification processes.

6.1 Objectivity of research

During the simulation part and especially during the system verification phase all the comparisons of the modal frequencies have been compared several times. This makes the system model in RoBeDyn as accurate as possible. Therefore, with these initial values the system model can be modeled again with same results.

Vibration analysis is mainly only a matter of plotting and RoBeDyn modeling. This means that if the system model is correct then the stability analysis will perform as well as in this study. However, designer needs to be careful because the control system affects to the place of the displacement peaks. Therefore, it needs to be evaluated right before vibration analysis. The correct control system can be seen from the vibration analysis diagram displacement peaks and from the stability analysis results.

The stability analysis fulfills the standard requirements and draws the correct shape for the sensitive response diagram. This, together with the vibration analysis diagrams, means that the control system is correct and it performs the given task well.

The touchdown test can be performed many different ways and the test itself is complex because it contains so many equations, which means that the time integration loop becomes long and difficult process. However, comparing the results to the standardized orbit responses given by ISO 14839-4 standard it can be said that the results of the study are similar.

Ultimately, it can be said that all the standardized AMB verifications are repeatable with different research methods and different user and if the goal is to repeat this study, the initial values, which are known for sure in this study, should be exactly the same. Moreover, from the simulation results it can be seen that they support each other, for example, if the rotor model is incorrect then touchdown test is impossible to do. Therefore, the results are unequivocal.

6.2 Reliability analysis

The reliability of the results are as accurate as concept level system simulation results can be, because, there are parameters that need to be measured from the real system. These parameters are the bearing friction, which have been estimated using the table values for metal-metal surface. This should be very close to real value but there are still questions about the reliability.

The second set of important parameters are in the safety bearing support elements that contains the stiffness, damping, and effective mass. All these three different parameter are dependent on each other and the relationship can be seen in chapter 4.3.3 ‘’Touchdown test’’. The connection between these means that it is crucial to get the first parameter, stiffness correct. In this study, these parameters are evaluated with SolidWorks and dynamic behavior evaluation methods, but to be certain about the answers they should be measured when the prototype is at the point of construction.

The third place where reliability should be questioned is in the area of human error. Since this study has been done by only one person, one mistake may repeat itself throughout the study. However, all places where this kind of error may occur have been verified with different simulation programs or different methods, but it is still a good point to keep in mind.

One issue in the reliability of the simulation program is that these results can be verified from real systems, but because this project is still at the concept level these measurements are not possible at this point. Therefore, these results are correct until different studies with more accurate initial values are conducted, and produce different results.

6.3 Value and Applications to new results

These new results will make the future AMB system verification process faster, more efficient, and more accurate than previously. This is because the system verifications methods are difficult to read from standard text, but in this study, the methods are listed and the instructions are given more clearly. Therefore, these methods are universal and are not bound to this specific system.

Other application of the study is that it contains easier data management, and everyone from mechanical designer to end user can find the most important parts of the system data from one specific standardized check list. This check list also makes good basic information packet for marketing because the vendor and possible end user can see all the details of the information and they can evaluate that the machinery is correct.

The final application is not universal but is specific to this project. This application contains the RoBeDyn system models that can be used for further calculations and simulations. Because the simulation model is complicated to perform it is a good idea to use the same model after it has been verified with more accurate initial values. This makes further calculation and simulation processes faster and more convenient.

6.4 Follow-up research

In future, these verifications need to be repeated with more accurate parameters. This will make the system model more accurate and more reliable for this specific application. After this the verification simulations will give better answers, and it can then be decided whether the machinery will pass the standardized test in real situation.

The second issue in the future that it would be good to study is the touchdown bearing tests. There should be one piece of research that deals only with the touchdown bearings and their behavior. This will make sure that the bearing models and the verifications are current. In addition this kind of research would help in developing process in the future because designers would have some basic level from which to start their own process.

7 SUMMARY AND CONCLUSIONS

The main objective of this study was to verify the exciting AMB system with standardized simulation methods given by the ISO 14839 and API 617 standards. This research project required fair amount of Matlab coding and some mathematical evaluation methods. Even though, this study contains a considerable number of plain standard text because the main focus is on the ISO 14829 standard.

The first steps contained the theoretical approach to the AMB system and the standard text. The importance here was on the different verification methods that are critical to the system and its running. These procedures included the vibration analysis and the system design such as clearances etc. The final two verification methods were the stability margin analysis and touchdown test. These can be done after the system is stable enough to run with maximum operation speed.

After the theory was introduced, the practical verification with RoBeDyn Matlab script was introduced. This process contained different steps:

- Collecting data from the AMB system 3D-model and from previous research.
- Processing and making the RoBeDyn data model from the collected data.
- Verifying the RoBeDyn model using modal frequencies from SolidWorks and RoBeDyn.

When the input model was ready, the actual simulations could be done by plotting the different parts of the model with RoBeDyn script. This method gave accurate results to the vibration analysis and stability margin test. However, the touchdown test could not be performed in at similar way because it needed more information about the backup bearing support elements, the backup bearings, and the rotor strength calculations. For these reasons the touchdown test could be the main subject in another study, but in this study the RoBeDyn script was simplified in a way that the backup bearing forces use linear stiffness and damping factors instead of nonlinear. This made the calculation process much faster with fewer equations and, nonetheless, the model is accurate. However, the script still required

parameters that do actually exist, so they needed to be evaluated. This evaluating was made with following steps:

- Calculate stiffness from the 3D strength analysis with a known force to obtain displacement
- From the modal frequencies and stiffness, the effective mass
- From the effective mass and stiffness, the critical damping
- Evaluating the damping ratio

Even if these parameters are accurate evaluations they should be at least checked when making follow-up research from these models.

After all the evaluating and simulation processes it can be seen that the PoC AMB system performed well in the standardized verification methods and clearly passed them. Therefore, it can be said that the study fulfilled its purpose given in the main goal section. The secondary goal was only partly fulfilled because the standardized design specification list could not be fully completed. This was simply because of a lack of information and these blank parts can be completed when the machinery will be ready and in its own working environment.

REFERENCES

API 617-2. 2002. Axial and Centrifugal Compressors and Expander-compressors for Petroleum, chemical and gas industry services – Part 2: Basic design. 7th edition. Washington DC: American Petroleum Institute. p. 2-28

API 617-4. 2002. Axial and Centrifugal Compressors and Expander-compressors for Petroleum, chemical and gas industry services – Annex 4F: Application considerations for active magnetic bearings. 7th edition. Washington DC: American Petroleum Institute. p. 4-45

Chen, W. J. & Gunter, E. J. 2005. Introduction to Dynamics of Rotor-Bearing Systems. 1st edition. Trafford publishing, Victoria. p. 486. ISBN 1-4120-5190-8

Genta, G. 2005, Dynamics of Rotating Systems. Springer, New York. p. 654. e-ISBN 0-387-20936-0.

Halminen, O. & Kärkkäinen, A. & Sopanen, J. & Mikkola, A. 2015 Active magnetic bearing-supported rotor with misaligned cageless backup bearings: A dropdown event simulation model. Mechanical System and Signal Processing. Published online 2014. URL: http://ac.els-cdn.com/S0888327014002246/1-s2.0-S0888327014002246-main.pdf?_tid=0835f51e-640f-11e4-9502-00000aab0f27&acdnat=1415097825_4660c9ad48ce9db18102b49ce6bca45b

Heikkinen, J. 2014. Masters of Science; Younger researcher, Lappeenranta University of Technology. Conversation 6.8.2014. Conversation partner Ville Hakonen.

Heikkinen, J. 2014. HS-EDEN – PoC laakerit [private e-mail]. Receiver: ville.hakonen@lut.fi (cc). Sent 1.9.2014, clock 12:07 (GMT +0300)

Hochschule Zittau/Görlitz University of Applied sciences [from www-page]. Updated 3.6.2014 [referred 3.6.2014]. URL: http://ipm.hszg.de/en/institute/publikationen/publikationen-ipm/article/simulation-based-design-method-of-active-magnetic-bearings-according-to-the-criterion-of-dynamic-sti.html

Hynynen, K.M. 2011. Broadband excitation in the system identification of active Magnetic bearing rotor systems. (Ph.D. thesis), Lappeenranta University of Technology, URL: http://urn.fi/URN:ISBN:978-952-265-153-2.

IEC 60721-4. 2002. Classification of environmental conditions – Part 4: Guidance for the correlation and transformation of the environmental condition classes of IEC 60721-3 to the environmental tests of IEC 60068. 1st edition. Genève: International Electrotechnical Commissions. p. 37

ISO 14839-1. 2002. Mechanical vibration – Vibration of rotating machinery equipped with active magnetic bearings – Part 1: Vocabulary. 1st edition. Genève: International Organization for Standardization. p. 30.

ISO 14839-2. 2004. Mechanical vibration – Vibration of rotating machinery equipped with active magnetic bearings – Part 2: Evaluation of vibration. 1st edition. Genève: International Organization for Standardization. p. 20

ISO 14839-3. 2006. Mechanical vibration – Vibration of rotating machinery equipped with active magnetic bearings – Part3: Evaluation of stability margin. 1st edition. Genève: International Organization for Standardization. p. 35

ISO 14839-4. 2012. Mechanical vibration – Vibration of rotating machinery equipped with active magnetic bearings – Part 4: Technical guidelines. 1st edition. Genève: International Organization for Standardization. p. 41

ISO 1940-1. 2003. Mechanical vibration – Balance quality requirements for rotors in a constant rigid state – Part 1: specifications and verification of balance tolerances. 2nd edition. Genève: International Organization for Standardization. p. 28

Jauhiainen, T. 2014. 3214-B-TVH angular contact ball bearing [private e-mail]. Receiver: ville.hakonen@lut.fi (cc). Sent 2.9.2914, clock 12:02 (GMT +0300)

Jeon, S. & Ahn, H.J. & Han, D.C. 2002. Model validation and controller design for Vibration suppression of flexible rotor using AMB. KSME International Journal, vol. 16, no. 2. p. 1583-1593.

Kalman, R. 1964. When is a linear control system optimal? Journal of Basic engineering – Transaction on ASME. Series D p. 51–60.

Khulief, Y.A., and Mohiuddin, M.A. 1997. On the Dynamic Analysis of Rotors Using Modal Reduction. Finite Elements in Analysis and Design. p. 41-55.

Kärkkäinen, A. 2007. Dynamic simulations of rotors during drop on retainer bearings. Ph.D. thesis, Lappeenranta University of Technology, URL: http://urn.fi/URN:ISBN:978-952-214-445-4

LUT news. 2013. Suurnopeustekniikasta uutta liiketoimintaa Lappeenrantaan [www-document] Published 2013, updated 20.11.2013 [referred 22.5.2014]. URL: http://www.lut.fi/uutiset/-/asset_publisher/h33vOeufOQWn/content/suurnopeustekniikasta-uutta-liiketoimintaa-lappeenrantaan

Lösch, F. 2002. Identification and Automated Controller Design for Active Magnetic Bearing Systems, (Ph.D. thesis), ETH Zurich, URL: http:// mecos.com/pdf/PHD_0004.PDF

NTN. 2010. Precision Rolling Bearings [www-document]. Illinois, updated 25.7.2012 [referred 24.9.2014]. URL: http://www.ntnamericas.com/en/website/documents/brochures-and-literature/catalogs/precision-all2260.pdf

Pyrhönen, J. & Jokinen, T. Hrabovcová, V. 2008. Design of Rotating electrical Machines. 1st edition. Wiley & Sons, Ltd, Wiltshire. p. 512. ISBN 978-0-470-69516-6

SKF Group, Deep groove ball bearings [from www-page]. Updated 2.9.2014 [referred 2.9.2014]. URL: http://www.skf.com/group/products/bearings-units-housings/ball-bearings/deep-groove-ball-bearings/single-row-with-solid-oil/index.html?prodid=1052270014

Schwitzer, G. & Maslen, E. H. Magnetic Bearings Theory, Design, and Application to rotating machinery. Springer, London, New York. p. 535. e-ISBN 978-3-642-00496-4

Skogestad, S. & Postlethwaite, I. 2005. Multivariable Feedback control: Analysis and Design. 2nd edition. Wiley, Ames. p. 608. ISBN 978-0-470-01167-6

Smirnov, A. 2012. AMB system for high-speed motors using automatic commissioning. (Ph.D. thesis), Lappeenranta University of Technology, URL: http://urn.fi/URN:ISBN:978-952-265-363-5

Swanson, E. E. & Maslen, E. H. & Li, G. & Cloud C. H. 2008. Rotordynamic design audits of AMB supported machinery. Proceedings of the Thirty-seventh Turbomachinery Symposium. [www-document]. Virginia, updated 17.9.2008 [referred 23.5.2014]. URL: http://turbo-lab.tamu.edu/proc/turboproc/T37/T37-TUT01.pdf

Valtanen, E. 2010. Tekniikan taulukkokirja. 18th edition. Genesis kirjat Oy, Mikkeli. p. 1176.

Yoon, S.Y. & Lin, Z. & Allaire, P.E. 2013. Control of Surge in Centrifugal Compressors by Active Magnetic Bearings. Springer, New York. p. 275. ISBN 978-1-4471-420-9

Zhang, J. & Karrer, N. 1995. IGBT Power Amplifiers for Active Magnetic Bearings of High SpeedMilling Spindles. IEEE IECON 21st International Conference on Industrial Electronics, Control, and Instrumentation. p. 596–601.

APPENDIX

APPENDIX I: Typical radial magnetic bearing sizing chart. (ISO 14839-4, 2012, p. 24-25)

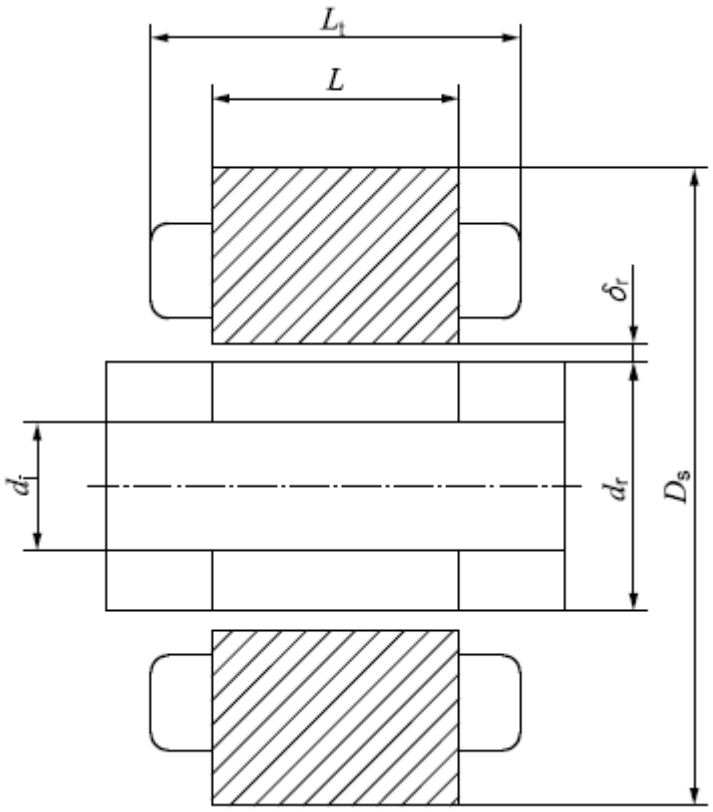

D_s mm	d_r mm	d_i mm	δ_r mm	$L_t - L$ mm	N_{max} r/min	F_0 N/mm/T^2	N_p
85	30	18	0,2	10,0	120 000	2,9	8
98	40	24	0,3	11,0	90 000	3,9	8
107	50	30	0,3	11,0	72 000	4,9	8
116	60	36	0,3	12,0	60 000	5,9	8
126	70	43	0,4	14,0	51 000	6,9	8
138	80	49	0,4	16,0	45 000	7,8	8
151	90	55	0,5	19,0	40 000	8,8	8
164	100	74	0,6	21,0	36 000	9,8	16
177	110	81	0,6	23,0	33 000	10,8	16
191	120	89	0,8	25,5	30 000	11,8	16
239	150	111	0,8	31,5	24 000	14,7	16
318	200	148	0,9	42,0	18 000	19,6	16
398	250	185	1,0	52,5	14 400	24,5	16
478	300	221	1,2	63,0	12 000	29,4	16

APPENDIX II: Typical thrust magnetic bearing sizing chart. (ISO 14839-4, 2012, p. 25-26)

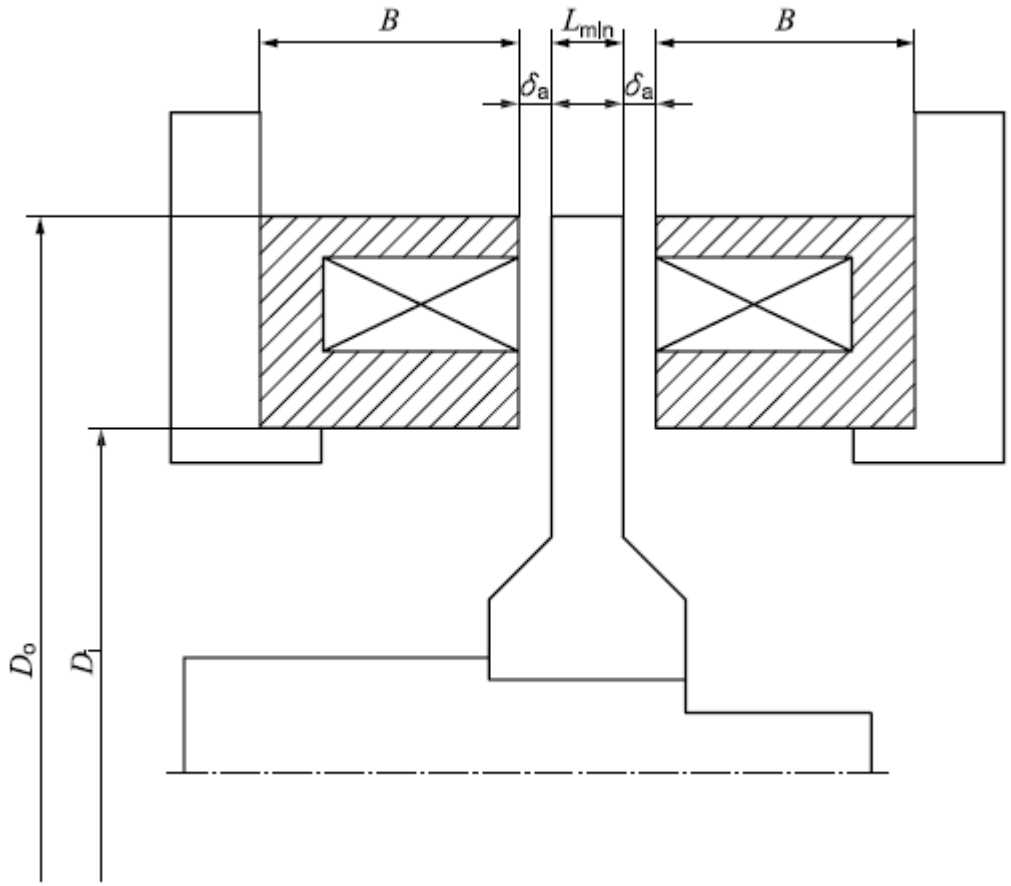

D_o mm	D_i mm	δ_a mm	B mm	L_{min} mm	N_{max} r/min	F N	N_p
46	24	0,3	17,0	4,0	115 000	50	2
60	31	0,3	21,0	5,0	89 000	200	2
85	44	0,3	25,0	7,0	61 000	500	2
150	78	0,4	50,0	20,0	33 000	4 000	2
200	106	0,4	62,0	27,0	24 000	8 400	3
300	156	0,5	65,0	35,0	16 000	15 700	3
400	208	0,6	69,0	30,0	12 000	24 300	3
500	260	0,6	82,0	35,0	9 500	38 400	3
600	310	0,8	94,0	40,0	7 500	56 000	3

APPENDIX III: Design specification check list. (ISO 14839-4, 2012, p. 28)

	Machine			
1	Type			
2	Customer			
3	End user			
4	New design/retrofit			
	General characteristics			
5	Operating speed range	r/min		
6	Nominal speed	r/min		
7	TRIP speed	r/min		
8	Orientation (horizontal/vertical/any)			
9	Power at nominal speed	kW		
10	Rotor weight	kg		
11	Rotor length	mm		
12	Balance quality	G		
13	Nature of process fluid			
	Machine environment			
14	Internal medium (air/vac/fluid)	Temp.:	°C, Pressure:	kPa
	Other info (composition/corrosive/humidity/etc.)			
	Available cooling medium (water/air/other/none)			
15	External medium (air/vac/fluid)	Temp.:	°C, Pressure:	kPa
	Other info (composition/corrosive/humidity/etc.)			
	Available cooling medium (water/air/other/none)			
16	Electronic cabinet environment	Temp.:	°C, Pressure:	kPa
	Distance to machine	m		
	Back-up batteries			
	Back-up time	min		
	Load definition			
17	Assembly drawing			
18	Static process load (radial)	N	Axial location:	mm
19	Static process load (thrust)	N	Axial location:	mm
20	Dynamic process load (radial)	N	Axial location:	mm
	Frequency	Hz		
21	Dynamic process load (thrust)	N	Axial location:	mm
	Frequency	Hz		
22	Additional dynamic load margin (radial)	N		
23	Additional dynamic load margin (thrust)	N		
	Touchdown bearing			
24	Supplied by (vendor/customer)			
25	Type (ball bearings/other)			
26	Mounting (resilient/hard)			
	Speed sensor			
27	Supplied by (vendor/customer)			
28	Type (Hall effect/optical/other)			

APPENDIX IV: Touchdown bearing clearance. (ISO 14839-4, 2012, p. 4)

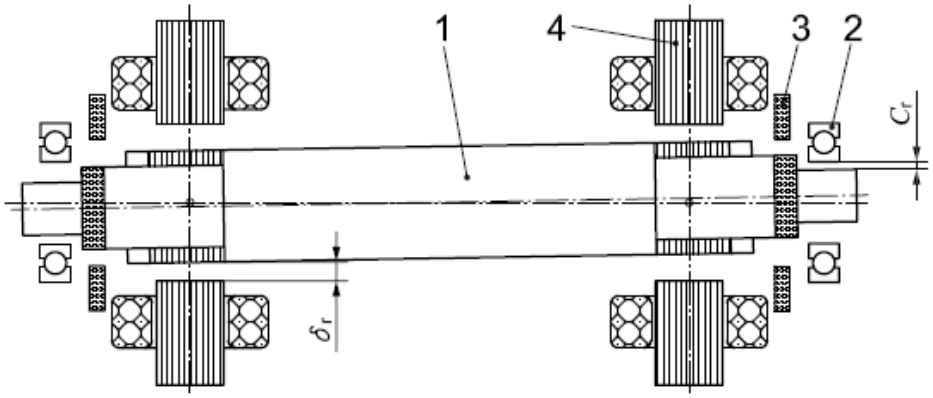

Key

1	shaft	$C_r \approx 0{,}5\delta_r$	
2	radial touchdown bearing	C_r	radial clearance
3	displacement sensor	δ_r	radial magnetic gap
4	radial magnetic bearing		

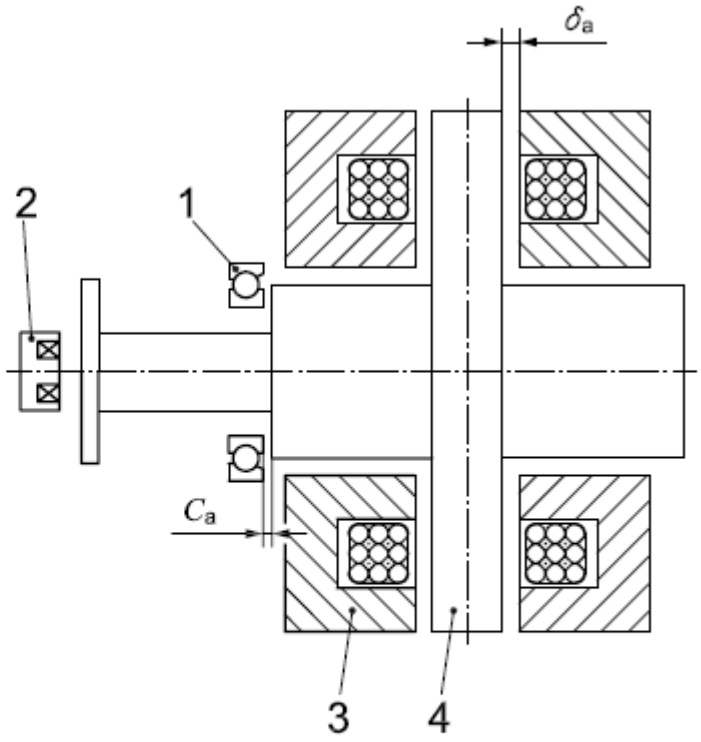

Key

1	thrust touchdown bearing	$C_a \approx 0{,}5\delta_a$	
2	thrust displacement sensor	C_a	axial clearance
3	thrust magnetic bearing	δ_a	axial magnetic gap
4	thrust disc		

APPENDIX V: Touchdown test rotor orbit responses. (ISO 14839-4, 2012, p. 19)

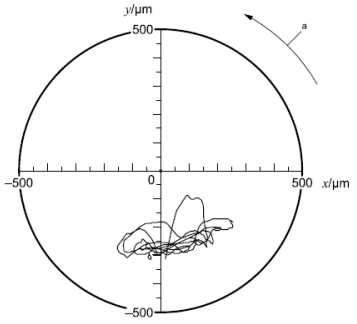

Key
x, y displacement
[a] Rotational direction.
NOTE Measurement duration is 0,2 s.

Ideal orbit response figure for touchdown test. Rotor is whirling at the bottom of the touch down bearing.

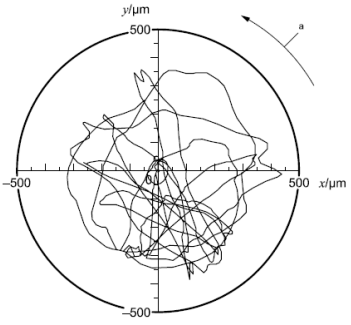

Key
x, y displacement
[a] Rotational direction.
NOTE Measurement duration is 0,2 s.

Chaotic bouncing are typical when damping of the bearing support is too low.

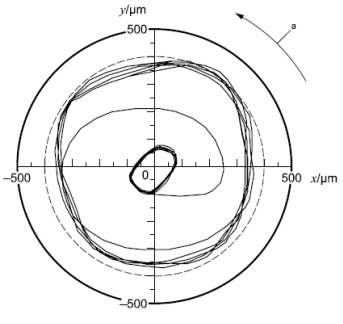

Key
x, y displacement
[a] Rotational direction.
NOTE Measurement duration is 0,2 s.

Backward or forward whirl response happens when static/dynamic force ratio is too high.